# Chromosome segregation and peptidoglycan remodelling are coordinated at a highly-stabilized septal pore to maintain bacterial spore development

Ahmed Mohamed[1], Helena Chan[1], Johana Luhur[1], Elda Bauda[2], Benoit Gallet[2], Cécile Morlot[2], Louise Cole[1,3], Milena Awad[4], Simon Crawford[5], Dena Lyras[4], David Z. Rudner[6], Christopher D. A. Rodrigues[1,#]

[1]The ithree Institute, University of Technology Sydney (UTS), Australia

[2]University of Grenoble Alpes, CNRS, CEA, IBS, Grenoble, France

[3]Microbial Imaging Facility (MIF), University of Technology Sydney (UTS), Australia.

[4]Infection and Immunity Program, Monash Biomedicine Discovery Institute and Department of Microbiology, Monash University, Melbourne, Australia

[5]Ramaciotti Centre for Cryo-Electron Microscopy, Monash University, Melbourne, Australia

[6]Department of Microbiology, Harvard Medical School, Boston, USA

## Summary

Asymmetric division, a hallmark of endospore development, generates two cells, a larger mother cell and a smaller forespore. Approximately, 75% of the forespore chromosome must be translocated across the division septum into the forespore by the DNA translocase SpoIIIE. Asymmetric division also triggers cell-specific transcription, which initiates septal peptidoglycan remodelling involving synthetic and hydrolytic enzymes. How these processes are coordinated has remained a mystery. Using *Bacillus subtilis*, we identified factors that revealed the link between chromosome translocation and peptidoglycan remodelling. In cells lacking these factors the asymmetric septum retracts, resulting in forespore cytoplasmic leakage and loss of DNA translocation. Importantly, these phenotypes depend on septal peptidoglycan hydrolysis. Our data support a model where SpoIIIE is anchored at the edge of a septal pore, stabilized by newly-synthesized peptidoglycan and protein-protein interactions across the septum. Together, these factors ensure coordination between chromosome translocation and septal peptidoglycan remodelling, to maintain spore development.
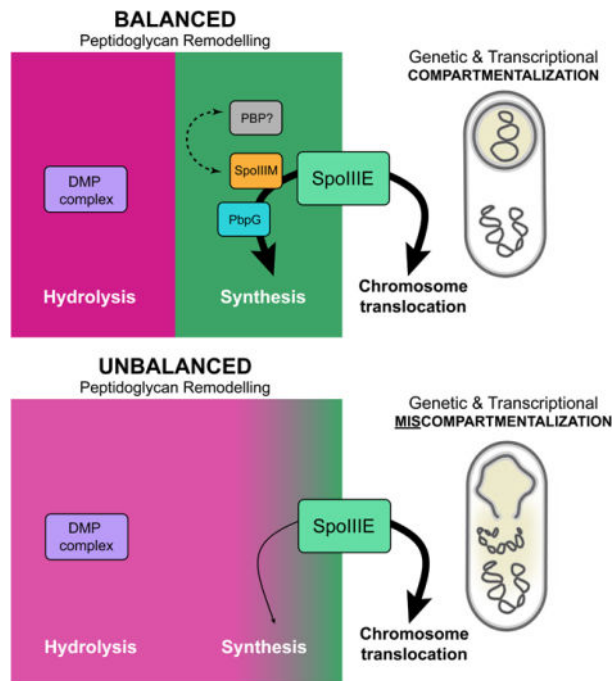
## Graphical Abstract

[#]corresponding author and lead contact: christopher.rodrigues@uts.edu.au, Tel: +61 (2) 9514-4066.

## Keywords

Development; Sporulation; Peptidoglycan; Chromosome Translocation

## Introduction

The establishment and maintenance of genetic and transcriptional compartmentalization during cytokinesis is a key aspect of development in all organisms. In eukaryotic cells, multiple lines of evidence suggest that proteins localized at the division site coordinate chromosome segregation with cytokinesis (Fraschini, 2020). This coordination requires interplay between the reorganization of the actin and microtubule cytoskeletal elements, a variety of motor proteins and membrane trafficking (Fraschini, 2020; Seiler and Justa-Schuch, 2010). In eukaryotic cells with a cell wall (e.g. yeast), cytokinesis also requires chitin synthases and hydrolytic enzymes such as chitinases and glucanases (Lesage and Bussey, 2006). Importantly, the molecular mechanisms governing coordination between chromosome segregation with cytokinesis remain poorly understood, even in the simplest organisms, such as bacteria. Here, using the bacterium *Bacillus subtilis* as a model system, we investigate the mechanisms underlying the coordination between chromosome translocation and the last steps in cytokinesis during sporulation, a primordial example of cellular development.

In dividing bacteria, genetic compartmentalization is achieved by segregating most of the chromosome into each daughter cell prior to cytokinesis. Here, a membrane-anchored DNA translocase of the broadly conserved FtsK/SpoIIIE family aids in the completion of chromosome segregation (Sherratt et al., 2010; Grainge, 2010; Barre, 2007). During endospore-formation in *Bacillus subtilis*, a more complex situation occurs: asymmetric

division generates two cellular compartments of different size and distinct developmental fates: a smaller cell called the forespore, that develops into the dormant spore, and a larger cell designated the mother cell (Stragier and Losick, 1996) (Fig. 1A). Importantly, asymmetric division precedes chromosome segregation and traps approximately 25% of the chromosome in the forespore, while the remaining 75% is translocated into the developing forespore by SpoIIIE (Wu and Errington, 1998; Sullivan et al., 2009) (Fig.1A). Remarkably, this occurs concomitantly with remodelling of the division septum and the early steps of spore envelope formation (Piggot and Hilbert, 2004). How these events are coordinated in a way that maintains transcriptional compartmentalization during development has remained unclear.

SpoIIIE is composed of three domains: an N-terminal transmembrane domain, a poorly conserved linker and a motor domain (Burton and Dubnau, 2010). The N-terminal transmembrane domain is required for SpoIIIE stability and localization to the middle of the asymmetric septum (Wu and Errington, 1997; Sharp and Pogliano, 1999; Sharp and Pogliano, 2002). The SpoIIIE motor domain contains three subdomains ($\alpha$, $\beta$, and $\gamma$), being classified as a member of the RecA family of ATPases and sharing ~78% sequence similarity to FtsK (Barre, 2007). $\alpha\beta$ assembles into a hexameric ring containing the ATPase machinery and a central channel through which double-stranded DNA is threaded (Cattoni et al., 2014). The SpoIIIE $\gamma$ domain translocates DNA directionally by recognizing chromosomal DNA sequence motifs called SpoIIIE Recognition Sequences (SRS) (Ptacin et al., 2008; Cattoni et al., 2013; Besprozvannaya et al., 2013).

Two proposed models explain how SpoIIIE translocates DNA across the septum (Fig. 1B & C). In the Aqueous Pore Model, SpoIIIE is anchored at the edges of a toroidal aqueous pore surrounded by an unfused septal membrane through which the chromosome is translocated (Wu and Errington, 1997; Fiche et al., 2013). In this model, the SpoIIIE motor domains are predominantly localized on the mother-cell side of the pore and the transmembrane domain is predicted to stabilize and coordinate septal pore closure with completion of chromosome translocation (Fiche et al., 2013). In the Membrane Channel Model, SpoIIIE exists on both sides of a fused septal membrane and its transmembrane domain forms intercellular channels through which the DNA is translocated (Burton et al., 2007; Yen Shin et al., 2015; Fleming et al., 2010). A lack of clear genetic evidence in support of either model has kept the debate surrounding these models open.

Concurrent with chromosome translocation into the forespore, compartment-specific sigma factors are activated to control gene expression in the mother cell and forespore. Upon asymmetric division, $\sigma^F$ is activated in the forespore (Fig. 1A), which controls a signal transduction pathway that triggers the activation of $\sigma^E$ in the mother cell (Piggot and Hilbert, 2004). $\sigma^E$ directs the synthesis of cell wall peptidoglycan (henceforth abbreviated as PG) hydrolases that assemble into the DMP complex (composed of SpoIID, SpoIIM and SpoIIP), which thin the septal PG and mediate engulfment of the forespore (Morlot et al., 2010; Chastanet and Losick, 2007) (Fig. 1D). In addition to PG degradation, engulfment is thought to involve PG synthesis by biosynthetic complexes, although these are yet to be defined (Ojkic et al., 2016). Upon completion of engulfment, membrane fission releases the forespore into the mother-cell cytoplasm as a protoplast surrounded by two membranes and

a thin layer of PG in between (Khanna et al., 2019; Tocheva et al., 2013; Doan et al., 2013). Finally, during engulfment a highly-conserved SpoIIIAH-SpoIIQ zipper-like interaction holds the mother cell and forespore membranes together and functions like a ratchet, promoting efficient, forward movement of the engulfing membranes (Broder and Pogliano, 2006; Ojkic et al., 2014) (Fig. 1D).

Here, we reveal that chromosome translocation and septal PG remodelling during engulfment are coordinated through an aqueous pore stabilized by the SpoIIIE protein itself, a protein called SpoIIIM (formerly YqfZ), septal PG synthesis by the forespore-specific PG synthase PbpG and by the SpoIIIAH-SpoIIQ interaction across the septal membrane (Fig. 7A). In the absence of these factors, the asymmetric septum retracts due to septal PG hydrolysis by the DMP complex, resulting in loss of cytoplasmic and chromosomal compartmentalization, and a block to spore development (Fig. 7C). Collectively, our work defines the coordination between septal PG remodelling and chromosome segregation that ensures genetic and cytoplasmic compartmentalization during spore morphogenesis and demonstrates the primordial importance of coordinating chromosome segregation with cytokinesis during development.

## Results

### A screen for synthetic lethal partners with *pbpG* identifies *spoIIIM*

The forespore produces two functionally redundant class A penicillin-binding proteins (PBPs), PbpG and PbpF, that generate a thin layer of spore PG called the germ cell wall (Fig. 1D) (McPherson et al., 2001). Sporulating cells lacking one of these proteins produce close to wild-type levels of spores; however, cells lacking both are severely impaired in sporulation (McPherson et al., 2001). Wild-type (henceforth WT) and the *pbpF* mutant produce forespores with an oblong-shape. However, sporulating cells lacking *pbpG* exhibit an abnormal, jellybean-like morphology (Fig. S1A) (Rodrigues et al., 2016). Based on this morphological difference, we hypothesized that PbpG and PbpF may have specialized roles and function in separate genetic pathways. To investigate this hypothesis and identify factors that function in each pathway, we used transposon-sequencing (Tn-seq) to screen for genes that become critical for sporulation in cells lacking either *pbpG* or *pbpF* (Meeske et al., 2016).

In validation of our genetic screen, *pbpF* was one of the top hits in the *pbpG* mutant transposon library and *pbpG* was one of the top hits in the *pbpF* transposon library (Fig. S1D & E). One of the strongest hits that was specific to the *pbpG* library was a gene called *yqfZ* that we have renamed *spoIIIM* (Fig. 1E and S1B). Previous work indicates that *spoIIIM* is transcribed in the mother cell compartment under σE control and encodes a 99 amino acid protein of unknown function (Eichenberger et al., 2003). SpoIIIM is predicted to have an N-terminal transmembrane segment and a C-terminal LysM domain (UniProt Consortium, 2018) that are implicated in binding to PG (Buist et al., 2008).

To verify that SpoIIIM becomes important for sporulation in *pbpG* cells, we determined the sporulation efficiency of *spoIIIM* and *spoIIIM pbpG* mutants (Fig. 1F). Consistent with previous reports, the *spoIIIM* mutant had a mild sporulation defect (76.6% spores)

and the *pbpG* mutant sporulated to near WT levels (87.3% spores). In validation of the Tn-seq screen, the sporulation efficiency of the *spoIIIM pbpG* double mutant was 8.8% (Fig. 1F). Expression of *spoIIIM* from an ectopic chromosomal locus restored sporulation efficiency of *spoIIIM* and *spoIIIM pbpG* mutants, to WT and *pbpG* levels, respectively (Fig. 1F). Finally, consistent with the results of the Tn-seq screen and in support of the idea that SpoIIIM is specifically required in cells lacking PbpG, no synergy was observed in the *spoIIIM pbpF* double mutant (Fig. S1C).

## PbpG and SpoIIIM are required for forespore morphology and compartmentalization

To begin to unravel how SpoIIIM and PbpG contribute to sporulation, we used fluorescence microscopy to determine if cells lacking these proteins exhibit morphological defects during development. Sporulating cells were imaged every 30 min after the onset of asymmetric division (1 hour and 30 minutes after the initiation of sporulation; T1.5). No obvious differences in forespore morphology were observed between the WT and *spoIIIM* mutant at early stages of development; however as the cells neared the completion of engulfment (T3) the *spoIIIM* mutant exhibited forespore morphologies that we categorized into four types: 1) WT-looking, 2) dwarf (small spherical forespores), 3) mislocalized (dwarf forespores positioned closer to the midcell of the mother cell) and 4) abnormal (forespores that lacked a spherical appearance and contained irregular membranes) (Fig. S2B & E). Consistent with the Tn-seq and sporulation efficiency data, the *spoIIIM pbpG* double mutant produced even more dwarf, mislocalized and abnormal forespores (Fig. S2E). Transmission electron microscopy (TEM) of *spoIIIM* and *spoIIIM pbpG* confirmed the presence of dwarf forespores with wrinkled membranes (Fig. S2F). Interestingly, closer inspection of *pbpG* cells revealed that 2.5% of the forespores have a dwarf phenotype (Fig. S2B & E), suggesting the absence of SpoIIIM enhances this defect.

The severity of the morphological defects in the *spoIIIM* and *spoIIIM pbpG* mutants led us to wonder if their forespores retain cytoplasmic compartmentalization. We engineered strains to express a cytoplasmic, cyan fluorescent protein (CFP) in the forespore under the control of a $\sigma^F$-dependent promoter ($P_{spoIIQ}$), and examined the distribution of the CFP signal by fluorescence microscopy during a sporulation time course (Fig. 1H). As expected, in WT cells the CFP signal was confined to the forespore throughout the entire time course (Fig. 1H). In the *spoIIIM* mutant we observed some cells with CFP signal confined solely to the forespore, some with stronger CFP signal in the forespore and weaker CFP signal in the mother cell and others with strong CFP signal throughout the entire sporangium (Fig. 1H). The frequency of *spoIIIM* sporulating cells with any CFP signal (weak or strong) in the mother cell increased over time and reached 33% at T3.5 (Fig. 1G). These observations suggest that *spoIIIM* forespores leak their cytoplasmic contents into the mother cell and loose compartmentalization. We observed an even higher proportion of miscompartmentalized sporulating cells in the *spoIIIM pbpG* double mutant (90% at T3.5) (Fig. 1G). Expression of *spoIIIM* in *trans* restored compartmentalization in the double mutant (Fig. S2A). Miscompartmentalization was also observed in the *pbpG* mutant, albeit at a low frequency (3%) (Fig. 1G & H). Highlighting the specific genetic relationship between *spoIIIM* and *pbpG*, the degree of miscompartmentalization of the *spoIIIM pbpF*

double mutant was comparable to the *spoIIIM* mutant (Fig. S2C & D). These data suggest that SpoIIIM and PbpG are also required for forespore compartmentalization.

Interestingly, miscompartmentalization and abnormal forespore morphology have both been reported for sporulating cells lacking *spoIIIE* (Liu et al., 2006; Hilbert et al., 2004; Doan, 2013). A side-by-side comparison of the *spoIIIM pbpG* double mutant and *spoIIIE* revealed similar forespore morphologies and degrees of miscompartmentalization (Fig. 1H & S2B). Furthermore, combining *spoIIIM* and/or *pbpG* with a hypomorphic allele of *spoIIIE* (SpoIIIE D584A) (Burton et al., 2007), which exhibits miscompartmentalization in a small fraction of cells, resulted in a dramatic increase in miscompartmentalization (Fig. S3A & B). These observations led us to investigate if the *spoIIIM* and *pbpG* mutant have other phenotypes in common with *spoIIIE*. Previous work demonstrated that *spoIIIE* miscompartmentalization can be suppressed when cells lack the engulfment hydrolases, SpoIID and SpoIIP (Hilbert et al., 2004). Sporulating cells lacking both SpoIID and SpoIIP have flat septa due to a block in septal PG hydrolysis (Fig. 1I) (Chastanet and Losick, 2007). In a *spoIID spoIIP* mutant, *spoIIIE* miscompartmentalization was almost completely abolished (Fig. 1J). Interestingly, this was also the case in *spoIIIM* and *spoIIIM pbpG* mutants (Fig. 1J), suggesting that SpoIIIE, SpoIIIM and PbpG help maintain compartmentalization, by counteracting the effects of PG hydrolysis during engulfment.

### SpoIIIM and PbpG are required for the dispersal of the SpoIIIE complexes

Based on the loss of compartmentalization in the *spoIIIE* mutant, it was previously hypothesized that the chromosome spanning the septum, and/or the absence of the SpoIIIE, creates an opening in the septum through which forespore cytoplasmic contents could leak (Hilbert et al., 2004; Liu et al., 2006). We considered the possibility that SpoIIIM and PbpG are required for SpoIIIE stability and in their absence SpoIIIE becomes unstable, generating this opening. To investigate this possibility, we examined the localization of a functional SpoIIIE-GFP fluorescent fusion (Burton et al., 2007), during a sporulation time-course in WT, *spoIIIM*, *pbpG* and *spoIIIM pbpG* mutant cells (Fig. 2). Consistent with previous work, in WT cells, SpoIIIE-GFP localizes in a discrete focus at the centre of the asymmetric septum (Fig. 2A & B) (Burton et al., 2007; Wu and Errington, 1997; Sharp and Pogliano, 1999). As cells progress through engulfment, the focus is often located in the engulfing membranes, and as engulfment nears completion, the focus disperses, with SpoIIIE-GFP localizing as diffuse signal in the forespore membranes (Fig. 2A, B & C). SpoIIIE-GFP dispersion is thought to represent detachment of SpoIIIE from the DNA (Ben-Yehuda et al., 2003). Consistent with this idea and previous reports (Sharp and Pogliano, 1999), the number of WT sporulating cells with foci declined over time (at T3.5, 35% of the cells had a SpoIIIE-GFP focus) (Fig. 2B & D). Importantly, SpoIIIE-GFP formed a discrete focus in *spoIIIM* and *spoIIIM pbpG* sporulating cells that resembled the focus observed in WT (Fig. 2B). Furthermore, quantification of SpoIIIE-GFP foci revealed similar signal intensities in WT and mutant strains (Fig. 2E). Thus, the miscompartmentalization in these mutants cannot be explained by instability of SpoIIIE. Interestingly, in the *spoIIIM* and *spoIIIM pbpG* mutants, the number of cells with SpoIIIE-GFP foci persisted for a longer period of time: at T3.5, 52% and 84% of the sporulating cells, respectively, contained a SpoIIIE-GFP focus (Fig. 2B & D). Thus, SpoIIIM and PbpG are required for SpoIIIE

dispersal into the forespore membranes. These results argue that forespore miscompartmentalization in cells lacking SpoIIIM and PbpG is not due to instability of SpoIIIE, suggesting these factors play a more direct role in maintaining compartmentalization at a septal pore.

### SpoIIIM and PbpG are required for efficient chromosome translocation and retention of the chromosome in the forespore

The data above suggest that SpoIIIE can still assemble into complexes in sporulating cells lacking SpoIIIM and PbpG. To investigate if SpoIIIE is capable of DNA translocation in the mutants, we used an approach based on the LacI-*lacO* system (Fig. 3A) and engineered strains to produce LacI-GFP under the control of the forespore reporter ($P_{spoIIQ}$-*lacI-gfp*) inserted at a chromosomal locus (*amyE*), present in the forespore at the time of asymmetric division (Wu and Errington, 1998; Marquis et al., 2008). These strains were also engineered to contain 48 *lacO* repeats at the *pelB* locus, which resides near the terminus (Fig. 3A). Using this approach, if the *pelB* locus is translocated into the forespore, a GFP focus will be observed in the forespore; if not, then no GFP focus will be observed (Fig. 3A). Due to miscompartmentalization in *spoIIIM* and *spoIIIM pbpG* mutants, we would also expect to observe some sporulating cells with a GFP focus bound to the mother cell chromosome, in addition to the one in the forespore (Fig. 3A). Furthermore, if cells fail to translocate the chromosome, we would expect to observe two GFP foci in the mother cell (Fig. 3A).

In WT sporulating cells, DNA translocation takes ~20 minutes (Burton et al., 2007). Accordingly, virtually all forespores contained a GFP focus at all time-points examined, indicating that the chromosome terminus was efficiently translocated into the forespore (Fig. 3B & C). In *spoIIIM* at T2, virtually all forespores (97%) contained a GFP focus, with a small fraction of cells containing two foci in the mother cell (3%) (Fig. 3C). This suggests that the majority of cells translocate the chromosome into the forespore in the absence of SpoIIIM. Interestingly, at T2.5 the number of cells with a GFP focus in the forespore decreased to 90%, while the number of cells with two GFP foci in the mother cells increased to 10%. A similar trend was observed at T3. These data suggest that in the absence of SpoIIIM the translocated chromosome is actively or passively effluxed back into the mother cell.

A similar but more dramatic trend was observed in the *spoIIIM pbpG* double mutant (Fig. 3B & C). At T2, the majority of the *spoIIIM pbpG* double mutant cells had translocated their chromosome (76% contained a GFP focus in the forespore). Remarkably, at T2.5 and T3, we observed a sharp decline in the number of cells with a GFP focus in the forespore and an increase in the number of cells with two mother cell foci (38% and 50% at T2.5 and T3, respectively) (Fig. 3B, C & E). Thus, most *spoIIIM pbpG* cells are capable of translocating a chromosome into the forespore but they fail to retain it. Finally, we note that while the vast majority of sporulating cells lacking PbpG successfully translocate a chromosome into the forespore, a small fraction of cells had two foci in the mother cell at T3 (2%) (Fig. 3B, C & E). Thus, even in the absence of *pbpG*, a small proportion of cells exhibit chromosome translocation defects.

Remarkably similar results were obtained when we examined chromosomes harboring the *lacO* array adjacent to origin at −7° (*yycR*) (Fig. 3D), at −120° (*yrvN*) or +87° (*yhdG*) (Fig. S3C & D). These results suggest that the entire forespore chromosome is effluxed into the mother cell in the absence of SpoIIIM and PbpG. Furthermore, analysis of origin-proximal (*yycR*) and terminus-proximal (*pelB*) loci in the *spoIIIM pbpG* cells, using different fluorescently-labeled DNA-binding proteins (LacI-YFP and TetR-CFP), revealed a pattern of YFP and CFP foci that is more consistent with passive efflux of the chromosome than active reverse translocation (Fig. S3E) (see Discussion). Collectively, these data suggest that the septal pore generated in sporulating cells lacking SpoIIIM and PbpG results in forespore chromosome loss, in addition to loss of its cytoplasmic contents.

## Impairing engulfment promotes compartmentalization and efficient chromosome translocation in cells lacking SpoIIIM and PbpG

Our data indicate that blocking engulfment PG hydrolysis almost fully restores compartmentalization to *spoIIIM* and *spoIIIM pbpG* cells. If forespore chromosome loss in these mutants is due to passive movement through a septal pore, blocking PG hydrolysis should similarly prevent chromosome loss from the forespore. This is indeed what we found. Sporulating cells lacking SpoIID and SpoIIP almost fully restored chromosome translocation, and retention, to the *spoIIIM* and *spoIIIM pbpG* mutants (Fig.4A). Furthermore, using a mutant (*spoIIB*) that impairs but does not abolish PG hydrolysis during engulfment (Perez et al., 2000) (Fig.4C), we found that both miscompartmentalization and forespore chromosome efflux were largely suppressed in the mutant backgrounds (Fig. 4B & C). Collectively, these data suggest that SpoIIIM and PbpG function to maintain compartmentalization of forespore cytoplasmic contents, including the chromosome, and counterbalance the activity of the PG hydrolases that remodel the septum during engulfment.

## Blocking chromosome translocation partially suppresses miscompartmentalization in cells lacking SpoIIIM and PbpG

Based on recent data showing that chromosome translocation into the forespore generates turgor pressure on the septal PG (Lopez-Garrido et al., 2018), we tested if chromosome translocation into the forespore contributes to miscompartmentalization in cells lacking SpoIIIM and PbpG. If so, a SpoIIIE mutant (*spoIIIE36*) that produces a stable SpoIIIE focus and does not impact compartmentalization but fails to translocate the chromosome (Sharp and Pogliano, 1999; Besprozvannaya et al., 2014), should suppress miscompartmentalization in cells lacking SpoIIIM and PbpG. Indeed, *spoIIIE36* partially suppressed miscompartmentalization in the *spoIIIM* and *spoIIIM* pbpG mutants (Fig. 4E & F). This result suggests that SpoIIIM and PbpG also function to counterbalance the effect chromosome translocation has on the septal pore.

## SpoIIQ is required for septal pore stability during engulfment in cells lacking PbpG, SpoIIIM or SpoIIIE

Since slowing down engulfment by reducing the efficiency of PG hydrolysis suppressed miscompartmentalization in the *spoIIIM* and *spoIIIM pbpG* mutants, we wondered if this would also be the case in sporulating cells lacking the SpoIIIAH-SpoIIQ zipper-like

interaction. As described in the introduction, this zipper-like interaction contributes to the efficiency of engulfment (Broder and Pogliano, 2006; Ojkic et al., 2014). To this end, we introduced the *spoIIQ* mutation into the *spoIIIM* and *pbpG* single mutants, and the *spoIIIM pbpG* double mutant backgrounds, and examined compartmentalization with our forespore reporter ($P_{spoIIQ}$-*cfp*) during a sporulation time-course (Fig. 5).

Surprisingly, instead of suppressing the compartmentalization defects, the *spoIIQ* mutant enhanced them. Among the sporulating cells with CFP signal, a subset appeared to completely lack a forespore compartment (Fig. 5B). Since $\sigma^F$ is required for the production of CFP and $\sigma^F$ only becomes active after asymmetric division, sporulating cells with this phenotype must have developed an asymmetric septum, which then retracted. Indeed, closer inspection of these cells revealed vestiges of septum formation (Fig. 5D). We refer to this phenotype as septal retraction (Fig. 5A). Quantification of septal retraction during a sporulation time course revealed that the phenotype increases over time (Fig. 5E) and represented 49% and 33% of the sporulating cells at T3, in the *spoIIQ spoIIIM* and *spoIIQ pbpG* double mutant, respectively. In the *spoIIQ spoIIIM pbpG* triple mutant, almost all cells (98%) displayed this phenotype by T3 (Fig. 5E).

Since the *spoIIIM pbpG* double mutant phenotypes closely resemble those in the *spoIIIE* mutant, we examined our forespore CFP reporter in the *spoIIQ spoIIIE* double mutant. Strikingly, the *spoIIQ spoIIIE* mutant had a similar frequency of septal retraction and vestiges of septa (Fig. 5B, D & E). Transmission electron microscopy confirmed the presence of retracted septa in the *spoIIQ spoIIIM pbpG* triple mutant and *spoIIQ spoIIIE* double mutant (Fig. S4A). Importantly, septal retraction in *spoIIQ spoIIIM* and *spoIIQ pbpG* double mutants or the *spoIIQ spoIIIM pbpG* triple mutant was not due to destabilization of SpoIIIE, as SpoIIIE-GFP still localized as foci in cells with retracted septa (Fig. S4B). In most cells with retracted septa, regardless of the mutant, SpoIIIE-GFP was observed as a single focus (Fig. S4B, C and D). Interestingly, in a small fraction of cells, two SpoIIIE-GFP foci were observed (Fig. S4B, C & D). Three-dimensional structured illumination microscopy (3D-SIM) confirmed these observations and suggest that SpoIIIE-GFP foci reside at the edges of an enlarged septal pore in the *spoIIQ spoIIIM pbpG* triple mutant (Fig. S4E & F).

Finally, we tested whether PG hydrolysis was required for septal retraction. In support of the idea that septal retraction requires PG hydrolysis, retraction was completely abolished and compartmentalization restored in all strains examined, that lack SpoIID and SpoIIP (Fig. 5C). Collectively, these data suggest that the septal membranes have not undergone fission at the time of chromosome translocation and that SpoIIIE, PbpG, SpoIIIM, and the zipper-like interaction between SpoIIIAH and SpoIIQ, all function to prevent the septal pore from enlarging during hydrolysis of the surrounding PG.

### Evidence that SpoIIIM, PbpG and SpoIIIE coordinate pore closure with completion of chromosome translocation

Building on the observations we describe thus far and taking advantage of the septal retraction phenotype, we tested the hypothesis that SpoIIIM and PbpG coordinate septal pore closure with completion of chromosome translocation. We hypothesized that

sporulating cells lacking SpoIIIM and/or PbpG are unable to coordinate septal pore closure with completion of chromosome translocation during engulfment PG hydrolysis, and if these cells also lack SpoIIQ, the membranes that line the pore, retract. We reasoned that if we hold back engulfment PG hydrolysis in the absence of SpoIIIM and PbpG, then the septal pore would have sufficient time to close and septal retraction will occur less frequently, unless chromosome translocation is yet to be completed and the septal pore is still open. This is indeed what we found, using the experimental system described in Figure S5A.

We performed this assay on strains that were otherwise WT, or lacked *spoIIQ* or both *spoIIQ* and *pbpG*. We induced the PG hydrolases at two time points after the onset of sporulation, T2 and T3, to give the cells different amounts of time to complete septal pore closure. At these time points, a similar proportion of the sporulating cells have two septa and CFP signal in the two forespore compartments (>86% for all strains) (Fig. S5A & E). Thus, after induction of the PG hydrolases, an increase in sporangia with CFP signal that have a single septum or lack septa would suggest septal retraction and failure to complete septal pore closure (i.e. membrane fission).

When the PG hydrolases were induced at T2 (Fig. S5B & C) and cells with CFP signal were examined one or 2 hours after induction (T3 & T4), most cells still had two septa and there was only a moderate increase in the number of cells with a single septum or no septa (i.e. the septa had retracted) in otherwise WT and *spoIIQ* cells. By contrast, in the *spoIIQ pbpG* double mutant cells, the proportion of cells with a single septum or no septa was much higher (Fig. S5G).

When the PG hydrolases were induced at T3 (Fig. S5D & SE) and cells with CFP signal were examined one or 2 hours after induction (T4 & T5), although the overall pattern of septal retraction between the strains was similar to when induction occurred at T2 (more septal retraction in *spoIIQ pbpG* cells, than in otherwise WT and *spoIIQ* cells), there was a reduction in the number of retracted septa for all strains (Fig. S5G). Thus, given sufficient time, the septal pore will undergo closure in the absence of SpoIIQ, PbpG and SpoIIIM.

Importantly, since *spoIIQ pbpG* sporulating cells have a higher frequency of retracted septa but a similar frequency of fully translocated chromosomes as otherwise WT, or *spoIIQ* sporulating cells at both time points of PG hydrolase induction (Fig. S5F & S5G), these data suggest that septal pore closure is delayed relative to completion of chromosome translocation in sporulating cells lacking SpoIIIM and PbpG.

Finally, we performed these experiments in the *spoIIQ spoIIIE* sporulating cells that do not translocate the forespore chromosome. Interestingly, the *spoIIQ spoIIIE* mutant behaved similarly to the *spoIIQ pbpG* mutant (i.e. septal retraction decreased when the PG hydrolases are induced at T3 (Fig. S5B–E & G). Thus, given sufficient time, the septal pore will undergo closure even in the absence of SpoIIIE (and in presence of untranslocated DNA) (Fig. S5F & H). This result establishes that SpoIIIE is not absolutely required for septal membrane fission.

## PG synthesis by PbpG is required for septal pore closure

Our data point to the possibility that PbpG contributes to PG synthesis around the septal pore, to maintain pore stability and drive pore closure. If this is the case, then the catalytic activity of PbpG should contribute to closure of the septal pore. To test this idea, we generated a mutant of PbpG (PbpG$^{E94A\ S365A}$, referred to as PbpG*) harbouring alanine substitutions at predicted catalytic residues in its glycosyltransferase and transpeptidase domains (Fig. S6A), in the context of a functional N-terminal, hexahistidine-tagged version of PbpG (His6-PbpG) (Fig. S6C). We note that PbpG* may still retain some residual catalytic activity, since it partially complemented the *pbpG* null allele in a *pbpG pbpF* (0.16%) (compared to 0.01% of the non-complemented *pbpG pbpF* double mutant) and *spoIIIM pbpG* double mutant background (57.4%) (compare Fig. S6C with Fig.1F). We examined the capacity of PbpG* to support septal pore closure by examining the different phenotypes reported thus far in the presence and absence of SpoIIIM: compartmentalization (Fig. 6A & S6D), SpoIIIE localization (Fig. 6C), chromosome translocation (Fig. 6B), and septal retraction (Fig. 6D & S6D). For all phenotypes tested, the catalytic activity of PbpG was required, although PbpG* produced phenotypes that were less penetrant than those observed in the *pbpG* null mutant, except in the case of SpoIIIE localization and septal pore retraction, where it phenocopied the *pbpG* null. Thus, PbpG itself, independent of its catalytic activity, is also required for the phenotypes described here. For reasons unknown, we were unable to detect His6-PbpG with His6 antibodies by immunoblot and thus confirm the levels of PbpG*. However, PbpG* in the context of a partially-functional but detectable, C-terminal, hexahistidine-tagged version of PbpG (PbpG-His6) produced similar levels of protein as the non-mutated counterpart (Fig. S6B). Thus, we conclude that PbpG catalytic mutations do not impact protein levels. Collectively, these results support the idea that PG synthesis by PbpG contributes to septal pore closure.

## SpoIIIM and PbpG interact with SpoIIIE

If SpoIIIM plays a role in septal pore closure, then it would likely localize to the septal membrane and exhibit a similar localization pattern as SpoIIIE. Consistent with the idea that SpoIIIM is anchored in the membrane and with its LysM domain surface-exposed, we found that a functional SpoIIIM-His6 fusion (Fig. S7C) was membrane-associated and susceptible to trypsin cleavage in a protease accessibility assay (Fig. S7A). To determine SpoIIIM's localization, we constructed a GFP-SpoIIIM fluorescent fusion and examined its localization over a sporulation time-course (Fig. 6E & F). GFP-SpoIIIM is fully-functional as the sole source of SpoIIIM in otherwise WT cells and partially functional in the absence of PbpG (Fig. S7C). In cells that had just begun engulfment, GFP-SpoIIIM localized as a faint septal focus or septal band (Fig. 6E). A similar localization pattern was observed at intermediate stages of engulfment (Fig. 6E). As engulfment neared completion, fewer cells had GFP-SpoIIIM signal (Fig. 6E & F). GFP-SpoIIIM localization was reminiscent of the dynamic localization of GFP-SpoIIIE, suggesting that SpoIIIM may depend on SpoIIIE for its localization. To test this, we examined GFP-SpoIIIM localization in *spoIIIE* over a sporulation time-course (Fig. 6E & F). In *spoIIIE*, we rarely observed GFP-SpoIIIM foci; instead most cells contained GFP-SpoIIIM septal bands (Fig. 6E). Furthermore, the frequency of cells with GFP-SpoIIIM signal in *spoIIIE* decreased earlier relative to WT cells (Fig. 6F).

To validate the localization relationship between SpoIIIE and SpoIIIM we took advantage of the *spoIIIE36* mutant, which, unlike SpoIIIE, fails to disassemble as engulfment nears completion but instead persists as a stable focus (Sharp and Pogliano, 1999). If SpoIIIM localization depends on SpoIIIE, then in the *spoIIIE36* mutant, GFP-SpoIIIM localization might also persist. We examined GFP-SpoIIIM localization in the *spoIII36* mutant, over a sporulation time-course (Fig. 6F). Quantification of the number of cells with GFP-SpoIIIM signal (focus and bands) in the *spoIIIE36* mutant, revealed that GFP-SpoIIIM foci persisted for a longer period of time (Fig. 6E & F). Similar observations, both in the *spoIIIE* and the *spoIIIE36* mutant background, were made in a merodiploid background using a stronger mother-cell promoter to drive GFP-SpoIIIM (Fig. S7D). Furthermore, immunoblot analysis of the SpoIIIM-His6 fusion confirmed that SpoIIIM stability depends on SpoIIIE (Fig. S7B). Collectively, these results suggest that SpoIIIM localization depends on SpoIIIE and these proteins form a complex *in vivo*.

To investigate if SpoIIIM and SpoIIIE interact directly, we used bacterial two-hybrid assays in *Escherichia coli*. In this assay, *E. coli* strain BTH101 expressed SpoIIIE and SpoIIIM fusions to domains T25 and T18 of *Bordetella pertussis* adenylate cyclase (Karimova et al., 1998). Positive interactions between SpoIIIE and SpoIIIM reunite T25 and T18 domains, resulting in *lacZ* expression, ß-galactosidase production and blue colonies on LB agar containing X-gal. We observed positive interactions, when T25 and T18 were fused to SpoIIIE and SpoIIIM (Fig. 6G). Interestingly, although PbpG appears to localize uniformly in the engulfing membranes (Ojkic et al., 2016), we also detected a positive interaction between PbpG and SpoIIIE (Fig. 6G). Collectively these results suggest that SpoIIIE, SpoIIIM and PbpG function together in maintaining PG synthesis around the septal pore during chromosome translocation, thereby ensuring compartmentalization in the face of septal PG hydrolysis.

## Discussion

Critical to a better understanding of the mechanisms coordinating cytokinesis with chromosome segregation during development is a detailed appreciation of these mechanisms in simpler organisms, such as bacteria. Our data demonstrate that coordination between cytokinesis and chromosome segregation during bacterial spore development requires an intricate balance between enzymatic remodelling of cell wall material, stabilization of the division septum and chromosome segregation. Our data indicate SpoIIIE, SpoIIIM and PbpG coordinate forespore chromosome translocation with septal PG remodelling, at a highly-stabilized septal pore (Fig. 7A & C). Our observations support a model in which SpoIIIE plays two critical roles during sporulation: (1) it translocates a copy of the chromosome into the forespore compartment and (2) it functions to maintain the septal pore through which the chromosome travels during engulfment. This second role is achieved by the recruitment of SpoIIIM and PbpG. Our data further suggest that PbpG synthesizes PG around the septal pore to counteract the activity of the PG hydrolases and SpoIIIM, and SpoIIIE itself, function to reinforce the pore through protein-protein and protein-PG interactions. Finally, we reveal an important role for the highly-conserved SpoIIIAH-SpoIIQ zipper-like interaction in the stabilization of the septal membrane surrounding the pore.

Together these factors maintain the septal pore and prevent its expansion due to the action of the septal PG hydrolases during engulfment (Fig.7C).

Septal PG degradation by the DMP complex plays a central role in driving engulfment (Khanna et al., 2020). However, as our data suggest, PG degradation must be counteracted to ensure the septal pore, where SpoIIIE translocates the forespore chromosome, does not expand. Our data indicate that SpoIIIE, along with PbpG and SpoIIIM, are critical for this process and suggest that they act, in part, by restoring PG surrounding the pore that is lost due to the action of the DMP complex (Fig.7B). This model is in keeping with data suggesting that remodelling of the septum during engulfment requires a balance between PG synthesis and hydrolysis (Ojkic et al., 2016) and with cryo-electron tomography data demonstrating changes in septal PG thickness before and after PG hydrolysis (Tocheva et al., 2013). Our data suggest that PbpG is responsible for localized septal PG synthesis and we hypothesize that SpoIIIE and SpoIIIM function to constrain the pore, possibly by recruiting or activating additional PG synthases in this region (Fig. 7B). Consistent with this idea, FtsW, an essential PG glycosyltransferase of the SEDS family, forms a focus in the middle of the septum at the time of asymmetric division (Burton et al., 2007).

A surprising phenotype we observed was the movement of the forespore chromosome back into the mother cell, in cells lacking SpoIIIM and PbpG (Fig. 3 and S3C & D). A similar phenotype was observed by Pogliano and co-workers in cells where SpoIIIE is targeted for degradation at the initiation of chromosome translocation (Lopez-Garrido et al., 2018). In this situation it was proposed that the chromosome is either passively expelled into the mother cell, to minimize the repulsive and hydration forces associated with packing the chromosome into the small forespore, or actively reverse translocated by SpoIIIE. Thus, it is possible that the movement out of the forespore reported here represents a similar scenario. Interestingly, we found that in cells lacking SpoIIIM and PbpG, SpoIIIE is not degraded but resides in active, stable complexes (Fig. 2). Thus, we have identified a condition where SpoIIIE is present and capable of translocating the chromosome into the forespore, but the chromosome fails to remain there. While it is tempting to hypothesize that PbpG and SpoIIIM normally function to prevent reverse translocation, we favor a simpler model in which these proteins prevent enlargement of the pore and passive efflux of forespore cytoplasmic content, and its chromosome, into the mother cell, during engulfment PG hydrolysis. In support of this model, chromosome efflux in the absence of PbpG and SpoIIIM is suppressed when engulfment PG hydrolysis is blocked or impaired (Fig. 4A and B).

An unexpected phenotype we identified in this study was that in actively engulfing cells lacking the highly-conserved SpoIIIAH-SpoIIQ zipper-like interaction and SpoIIIE, or SpoIIIM, or PbpG (or both), the asymmetric septum forms (and $\sigma^F$ is activated), but then retracts, abolishing development (Fig.5 & S4A). The SpoIIIAH-SpoIIQ zipper-like interaction has been shown to be particularly important in sporulating cells where the PG is degraded by lysozyme (Broder and Pogliano, 2006; Blaylock et al., 2004). Similarly, we hypothesize that it also functions to prevent the septal membranes from retracting during septal PG hydrolysis. As hypothesized above, in the absence of SpoIIIE, SpoIIIM or PbpG there is reduced PG synthesis and destabilization of the septal pore. The reduced PG

synthesis, combined with the thinning of septal PG at the onset of engulfment and the decreased membrane stability occurring in the absence of SpoIIIAH-SpoIIQ zipper, likely leads to progressive pore enlargement as the DMP complex makes its way outwards from the middle of the septum. Consistent with this hypothesis, we show that septal retraction can be prevented by blocking engulfment PG hydrolysis (Fig. 5C).

Overall, our results provide a more complete picture of how bacteria differentiate into spores, a morphological process that involves an asymmetric septum with a pore that must coordinate multiple developmental processes at once: the translocation of a chromosome across it, the maintenance of compartmentalization and the dramatic remodelling of the forespore envelope. More broadly, we show how coordination of different processes is critical to the establishment and maintenance of genetic and transcriptional compartmentalization during cytokinesis, key aspects of development and differentiation in all organisms. Finally, our results highlight the importance of modern approaches in genetics for distinguishing between disparate biological models.

## STAR Methods

### RESOURCE AVAILABILITY

**Lead Contact—**Further information and requests for resources and reagents should be directed to and will be fulfilled by the Lead Contact, Christopher Rodrigues (christopher.rodrigues@uts.edu.au).

**Materials Availability—**All materials generated in this study are available from the Lead Contact without restriction.

**Data and Code Availability—**The datasets generated during this study are available upon request from the Lead Contact.

### EXPERIMENTAL MODEL AND SUBJECT DETAILS

**Bacterial Strains and Growth Conditions—**All *B. subtilis* strains used in this study were derived from strain 168 or PY79. *B. subtilis* cells were induced to sporulate via resuspension at 37°C according to the Sterlini-Mandelstam method or through exhaustion of nutrients in supplemented Difco Sporulation medium (DSM). Deletion mutant strains were either obtained from the *B. subtilis* Single Gene Deletion Library (Addgene) (Koo et al., 2017) or from pre-existing strains in the laboratory. All BKE mutants were back-crossed into *B. subtilis* 168 before assaying and prior to antibiotic cassette removal. Antibiotic cassette removal was performed using a temperature-sensitive plasmid that constitutively expresses Cre recombinase. Genetic constructs were obtained from previously existing *B. subtilis* strains found within the laboratory or through restriction enzyme-based cloning of PCR products into ectopic-integration, double-crossover plasmid vectors that were then transformed into *B. subtilis.* Tables of strains (Table S1), plasmids (Table S2), oligonucleotide primers (Table S3) can be found in the Supplemental Information.

## METHOD DETAILS

**Sporulation efficiency assays—**Sporulation efficiency was examined using the heat-kill assay of 24–30-hour grown cultures, where the total number of heat-resistant (80°C for 20 min) colony forming units (CFUs) was compared to wild-type heat-resistant CFUs.

**Transposon Insertion Sequencing—**Transposon insertion sequencing (Tn-seq) was performed on WT (bDR2413) *pbpG* (bCR1557) and *pbpF* libraries (bCR1558), as described previously (Meeske et al., 2016). About 750,000 transformant colonies were harvested, aliquoted, and frozen. The aliquot culture was thawed on ice, resuspended in DSM, and diluted into 50 mL DSM at an OD600 of 0.05. Samples were collected at T24. The T24 samples were incubated at 80°C for 20 minutes to kill sporulation-defective cells and then plated to on LB agar allow gemination and outgrowth. Approximately, 750,000 colonies were harvested and their genomic DNA extracted and digested with MmeI enzyme to cut the MmeI restriction site inserted at the inverted repeat sequences of the magellan6 transposon. Barcode adapters were ligated and the transposon-chromosome junctions were amplified by PCR using 16 cycles. PCR products were gel-purified and sequenced on the Illumina HiSeq platform using TruSeq reagents (Tufts University TUCF Genomics facility). Reads were mapped to the *B. subtilis* 168 genome (NCBI NC_000964.3), tallied at each TA site.

**Fluorescence Microscopy—**Live-cell fluorescence imaging was performed by placing cells on a 2% (w/v) agarose pad prepared in resuspension medium and set using a gene frame (Bio-Rad). When sporulating cells reached the desired time-point, 200 μL of the culture was pelleted by centrifugation, and then resuspended in 10 μL of resuspension medium containing the membrane dye TMA-DPH (1-(4-trimethylammoniumphenyl)-6-phenyl-1,3,5-hexatriene *p*-toluenesulfonate) (0.05 mM) or FM 4–64 (*N*-(3-Triethylammoniumpropyl)-4-(6-(4-(Diethylamino) Phenyl) Hexatrienyl) Pyridinium Dibromide) (0.67 μg/μL). After gentle vortexing, 2 μL of the cell suspension was spread on the agarose pad, and a coverslip was placed on top of the gene frame. Cells were imaged by standard epifluorescence microscopy using a Zeiss Axioplan 2 Microscope equipped with 100x objective N/A 1.4. A DAPI filter to excite the TMA-DPH membrane dye with an exposure time of 400 ms. CFP, GFP, and YFP filters were used with exposure times of 600 ms, 800 ms, and 1000 ms, respectively. 3D-structured illumination microscopy was performed using the DeltaVision OMX SR microscope equipped with Olympus PlanApo N 60x objective lens N/A 1.42. The 1.515 immersion oil was selected after calculating the refractive index using softWoRx software. mCherry/A568 and GFP/A488 filters were used with exposure times of 15–20 ms and 10–15% intensity (%T).

**TEM imaging—**For the images in Figure S2F, sporulating cells were pelleted in 1.5-mL Eppendorf tubes at 10,000 rpm for 3 min and placed into primary fixative, consisting of 2.5% glutaraldehyde in 0.1 M sodium cacodylate buffer, for 2 h at room temperature. The cells were rinsed in fresh sodium cacodylate buffer three times for 15 min each. Secondary fixation was performed using 1% osmium tetroxide and 1.5% potassium ferricyanide in cacodylate buffer for 1 h at room temperature. The cells were then rinsed in three washes of Milli-Q water for 15 min each. The fixed cell pellets were dehydrated by incubating in

increasing concentrations of ethanol for 15 min, consisting of 30, 50, 70, 90 and 100% ethanol. Dehydrated cell pellets were incubated in a mixture of LR White resin and ethanol at a ratio of 1:1 for 6 h at room temperature, followed by a 2:1 LR White/ethanol mixture overnight. Cell pellets were incubated in 100% LR White resin for 6 hours, followed by another 100% resin change overnight. The cell pellets were then placed into gelatin capsules in 100% resin and the resin polymerised for 24 h in an oven at 60°C. Resin embedded tissue was sectioned with a Diatome diamond knife using a Leica UCS ultramicrotome. Sections of thickness 70 – 90 nm were collected onto formvar-coated 100 mesh copper grids and stained sequentially with 1% uranyl acetate for 10 min and lead citrate for 5 min. The sections were imaged in a JEOL 1400+ transmission electron microscope at 80kV, and images captured with a digital camera at a resolution of $2K \times 2K$.

For the images in Figure S4A, Sporulating cells were harvested by centrifugation at $3,220 \times$ g for 10 min. The cell pellet (1.4 μL) was dispensed on the 200-μm side of a type A 3-mm gold platelet (Leica Microsystems), covered with the flat side of a type B 3-mm aluminum platelet (Leica Microsystems), and was vitrified by high-pressure freezing using an HPM100 system (Leica Microsystems). Following freeze-substitution at −90°C for 80 h in acetone supplemented with 1% OsO4, the samples were warmed up slowly (1°C/h) to −60°C (AFS2; Leica Microsystems). After 8 to 12 h, the temperature was raised (1°C/h) to −30°C, and the samples were kept at this temperature for another 8 to 12 h before being rinsed 4 times in pure acetone. The samples were then infiltrated with gradually increasing concentrations of resin (Embed812, EMS) in acetone (1:2, 1:1, 2:1 [v/v]) for 3 h while raising the temperature until 20°C. Pure resin was added at room temperature. After polymerization at 60°C, 80-nm-thin sections were obtained using an ultramicrotome UC7 (Leica Microsystems) and were collected on formvar-carbon-coated 100-mesh copper grids. The thin sections were post-stained for 5 min with 5% aqueous uranyl acetate, rinsed, and incubated for 2 min with lead citrate. The samples were observed using a CM12 (Philips) or Tecnai G2 Spirit BioTwin (FEI) microscope operating at 120 kV with an Orius SC1000B CCD camera (Gatan).

**Immunoblot Analysis—**Whole-cell lysates from sporulating cells were prepared as previously described (Rodrigues et al., 2016). Samples were heated for 15 min at 50°C prior to loading. Equivalent loading was based on OD600 at the time of harvest. Samples were separated on a 12.5% polyacrylamide gel and transferred to a PVDF membrane. Membranes were blocked in 5% non-fat milk with 0.5% Tween-20 for 1 h. Blocked membranes were probed with anti-His (1:4000) (Genscript), anti-SpoIIIAG (1:10000) (Doan et al., 2009) or anti-FtsZ (1:30000) (Hajduk et al., 2019) primary antibodies diluted into PBS with 5% non-fat milk (w/v) with 0.05% Tween- 20 at 4°C overnight. Primary antibodies were detected with horseradish-peroxidase conjugated anti-mouse or anti-rabbit antibodies (BioRad) and detected with Western Lightning ECL reagent as described by the manufacturer.

**Protease accessibility assay—**Protease accessibility assays were performed in sporulating cells lacking the SpoIIQ (Q) protein to ensure that the membrane proteins present in the inner and outer forespore membranes would not be artificially inaccessible because of protoplast engulfment (Broder and Pogliano, 2006). Twenty-five milliliters of sporulating cells (induced by resuspension) were harvested by centrifugation at hour 2.5

after the onset of sporulation, washed, and resuspended in 2 mL 1X SMM buffer (0.5 M sucrose, 20 mM MgCl$_2$, 20 mM maleic acid, pH 6.5). The cells were protoplasted by lysozyme (5 mg/mL final concentration) for 10 min with slow agitation. The protoplasts were harvested by centrifugation and resuspended in 1 mL of 1X SMM. Protoplasts (100 μL) were incubated with trypsin (30 μg/mL final concentration) (Worthington), trypsin and Triton X-100 (2% final concentration), or 1X SMM for 30 min at 30°C. Reactions were terminated by the addition of 100 μL of 2X SDS-sample buffer and incubation for 5 min at 95 °C. Five microliters from each reaction were analyzed by immunoblot.

## Plasmid construction

**pAT001a [*ycgO::spoIIIM (spec)*]:** pAT001a [*ycgO::spoIIIM (spec)*] was generated in a two-way ligation with *Eco*RI-*Bam*HI PCR product containing the *spoIIIM* gene (oligonucleotide primers oAT001 & oAT002 and 168 genomic DNA as template) and pKM083 cut with *Eco*RI-*Bam*HI. pKM083 (*ycgO::spec*) is an ectopic integration vector for double crossover integration at the non-essential *ycgO* locus.

**pAT003a [*ycgO::PspoIIIM-opt$_{RBS}$-gfp-spoIIIM (spec)*]:** pAT003a [*ycgO::PspoIIIM-opt$_{RBS}$-gfp-spoIIIM (spec)*] was generated in a three-way ligation with a *Hind*III-*Xho*I PCR product containing *opt$_{RBS}$-gfp* (oligonucleotide primers oAT005 & oAT006 and pCR227 DNA as template), and an *Xho*I-*Bam*HI PCR product containing the *spoIIIM* gene (oligonucleotide primers oAT007 & oAT002) with pAT002a (*ycgO::PspoIIIM*) as template cut with *Hind*III and *Bam*HI. pCR227 [*yhdG::PgerM-gerM-gfp*] (cat) contains *gfp* (C. Rodrigues - laboratory stock).

**pAT024a [*ycgO::PspoIID-opt$_{RBS}$-gfp-spoIIIM (spec)*]:** pAT024a [*ycgO::PspoIID-opt$_{RBS}$-gfp-spoIIIM (spec)*] was generated in a two-way ligation of an *Eco*RI-*Hind*III digest product from pCR113 containing *P$_{spoIID}$*, into an *Hind*III-*Bam*HI digest product of pAT003a (*ycgO::PspoIIIM-opt$_{RBS}$-gfp-spoIIIM*). pCR113 [*ycgO PspoIID malE (cat)*] contains the P*spoIID* promoter (C. Rodrigues - laboratory stock).

**pAT032a [*ycgO::PspoIIIM-spoIIIM-His6 (spec)*]:** pAT032a [*ycgO::PspoIIIM-spoIIIM-His6 (spec)*] was generated in a two-way ligation with *Eco*RI-*Bam*HI PCR product containing the *spoIIIM* gene with a C-terminal hexahistidine tag (oligonucleotide primers oAT001 & oCR659 and 168 genomic DNA as template) and pKM083 cut with *Eco*RI-*Bam*HI. pKM083 (*ycgO::spec*) is an ectopic integration vector for double crossover integration at the non-essential *ycgO* locus.

**pAT057a [*pelB::spoIIIE-GFP (cat)*]:** pAT057a [*pelB::spoIIIE-GFP (cat)*] was generated in a three-way ligation with a *Eco*RI-*Xho*I PCR product containing *spoIIIE* (oligonucleotide primers oCR694 & oCR695 and bBB042 DNA as template), and an *Xho*I-*Bam*HI PCR product containing *gfp* (oligonucleotide primers oCR696 & oCR697) with pKM020 (*pelB::tet*) as template cut with *Eco*RI and *Bam*HI.

**pAT090 [*ycgO::spoIIIE36 (tet)*]:** pAT090 [*ycgO::spoIIIE36 (tet)*] was generated in a two-way ligation with an *Eco*RI-*Bam*HI PCR product containing *spoIIIE36* (oligonucleotide

primers oCR694 & oCR717 and bBB069 DNA as template) with pKM086 (*ycgO::tet*) cut with *Eco*RIand *Bam*HI.

**pCR20a [*amyE::PspoIIQ-spoIVF_{RBS}-lacI-gfp (spec)*]:** pCR20a [*amyE::PspoIIQ-spoIVF_{RBS}-lacI-gfp (spec)*] was generated in a three-way ligation with *Hind*III-*Xho*I digest product containing *spoIVF_{RBS}-lacI* (oCR416 & oCR417 and bXW1200 DNA as template), *Xho*I-*Bam*HI digest product containing *gfp* (oCR418 and oCR353 and pCR154 as template) and pCR154 (amy*E::PspoIIQ-opt_{RBS}-gfp (spec)* (C. Rodrigues - laboratory stock) cut with *Hind*III-*Bam*HI.

**pJL013 [*pelB::spoIIIE36 (tet)*]:** pJL013 [*pelB::spoIIIE36 (tet)*] was generated in a two-way ligation with an *Eco*RI-*Bam*HI digest product containing *spoIIIE36* from pAT090 (*ycgO::spoIIIE36*) with pKM033 (*pelB::tet*) as template cut with *Eco*RIand *Bam*HI.

**pHC3 [*ycgO::PspoIIQ-opt_{RBS}-pbpG-His6 (tet)*]:** pHC3 [*ycgO::PspoIIQ-opt_{RBS}-pbpG-His6 (tet)*] was generated in a two-way ligation with *Hin*dIII-*Bam*HI PCR product containing the *pbpG* gene [oligonucleotide primers oAT139 & oAT160 and 168 genomic DNA as template] and pCR008 cut with *Hind*III and *Bam*HI. pCR008 [*ycgO::PspoIIQ-opt_{RBS}-gfp-spoIIQ (tet)*] contains the P*spoIIQ* promoter (C. Rodrigues - laboratory stock).

**pHC23 [*ycgO::PspoIIQ-opt_{RBS}-pbpG-His6 (E94A, S365A) (tet)*]:** pHC23 [*ycgO::PspoIIQ-opt_{RBS}-pbpG-His6 (E94A, S365A) (tet)*] was generated by sequential rounds of site-directed mutagenesis of pHC3 using oligonucleotide primers oAT96 & oAT97 to introduce the E94A mutation, followed by oAT147 & oAT148 to introduce the S365A mutation.

**pHC28 [*P_{lac}::T18-spoIIIE (amp)*] and pHC32 [*P_{lac}::T25-spoIIIE (kan)*]:** pHC28 [*P_{lac}::T18-spoIIIE (amp)*] and **pHC32** [*P_{lac}::T25-spoIIIE (kan)*] were generated in a two-way ligation with *Xba*I-*Bam*HI PCR product containing the *spoIIIE* gene [oligonucleotide primers oCR716 & oCR717 and 168 genomic DNA as template] and pUT18C and pKNT25 (Karimova et al., 1998) , respectively, cut with *Xba*I and *Bam*HI.

**pHC29 [*P_{lac}::T18-spoIIIM (amp)*] and pHC33 [*P_{lac}::T25-spoIIIM (kan)*]:** pHC29 [*P_{lac}::T18-spoIIIM (amp)*] and **pHC33** [*P_{lac}::T25-spoIIIM (kan)*] were generated in a two-way ligation with *Xba*I-*Bam*HI PCR product containing the *spoIIIM* gene [oligonucleotide primers oCR718 & oCR719 and 168 genomic DNA as template] and pUT18C and pKNT25 (Karimova et al., 1998) , respectively, cut with *Xba*I and *Bam*HI.

**pHC30 [*P_{lac}::T18-pbpG (amp)*] and pHC34 [*P_{lac}::T25-pbpG (kan)*]:** pHC30 [*P_{lac}::T18-pbpG (amp)*] and **pHC34** [*P_{lac}::T25-pbpG (kan)*] were generated in a two-way ligation with *Xba*I-*Bam*HI PCR product containing the *pbpG* gene [oligonucleotide primers oCR720 & oCR721 and 168 genomic DNA as template] and pUT18C and pKNT25 (Karimova et al., 1998), respectively, cut with *Xba*I and *Bam*HI.

#### Other constructs

**[*ycgO::PpbpG-his6-pbpG (erm)*] and [*ycgO::PpbpG-his6-pbpG$^{E94A,S365A}$ (erm)*]:** *Hind*III-*PpbpG* was amplified by oAT137 and oHC056 using168 genomic DNA as template. The *his6-pbpG-Xho*I and *his6-pbpG$^{E94, S365A}$-Xho*I DNA fragments were amplified by oHC055 and oCR704 using pHC3 and pHC23 as templates respectively. *Hind*III-*PpbpG* and *his6-pbpG-Xho*I and similarly *Hind*III-*PpbpG* and *his6-pbpG$^{E94,S365A}$-Xho*I were ligated by Isothermal assembly using oHC055 and oHC056 to generate and then ligated into pKM084 (*ycgO::erm*) as template cut with *Hind*III and *Xho*I. Finally, after ligation into pKM084, the two constructs were transformed directly into *B. subtilis*.

## QUANTIFICATION AND STATISTICAL ANALYSIS

**Sporulation Efficiency Analysis**—All the sporulation efficiency data are average (± SD) of 3 biological replicates.

**Tn-seq Analysis**—Mapped genes in which reads were statistically underrepresented were identified using the Mann Whitney U test. Visual inspection of transposon insertion profiles was performed with the Sanger Artemis Genome Browser and Annotation tool.

**Image Analysis**—Microscopy images were processed by adjusting the brightness and contrast using the Fiji software (Schindelin et al., 2012). All quantifications were performed using the manual counting tool of the Fiji software, and the raw data was then exported into Excel for data collation and graph generation. At least two fields of view (90.13 × 67.53 μM) were acquired for each biological replicate and contained hundreds of cells, each. The criteria described below, or in results and legends, was used to quantify each phenotype.

- Quantification of forespore miscompartmentalization (Fig. 1G, 4E, 6A, S2D & S3B and): any cell with forespore-expressed CFP signal in the mother cell was classified as miscompartmentalized. The percentage of miscompartmentalized cells (average frequency ± SD of 3 biological replicates) was calculated based on the total number of sporulating cells that had progressed into the asymmetric division stage of development and contained CFP signal. *n*>750 per time-course, per strain, per replicate.

- Quantification of chromosome translocation using the LacI-GFP / *lacO* system (Fig. 3C & D, 4A & B, 6B, S3C & D): we followed the criteria described in Figure 3A and the percentage of cells (average frequency ± SD of 3 biological replicates) was calculated based on the total number of sporulating cells that contained a GFP focus and had progressed into or beyond asymmetric division. *n*>600 per time-course, per strain, per replicate.

- Quantification of chromosome translocation using the dual reporter system (TetR-CFP/ *tetO* & LacI-YFP/ *lacO*): we followed the criteria described in Figure S3E and the percentage of cells (average frequency ± SD of 3 biological replicates) was calculated relative to the total number of sporulating cells that contained four foci, two CFP foci and two YFP foci. Not all cells contained four visible foci within the plane of view during development: the four foci were

clearly visible in approximately 25%, 30% and 47% of the sporulating cells, at T2, T2.5 and T3 respectively. n>30 per time-point, per replicate.

- Quantification of septal retraction (Fig. 5E & 6D): any cell with forespore-expressed CFP signal in the mother cell and a non-continuous asymmetric septum, or vestiges of an asymmetric septum (based on the membrane signal), was classified as having a retracted septum. The percentage of cells with retracted septa (average frequency ± SD of of 3 biological replicates) was calculated based on the total number of sporulating cells that had progressed into or beyond asymmetric division. $n$>600 per time-point, per strain, per replicate.

- Quantification of cells with a SpoIIIE-GFP focus (Fig. 2D & 6C): the percentage of cells with a SpoIIIE-GFP focus (average frequency ± SD of of 3 biological replicates) was calculated based on the number of sporulating cells that contained a GFP focus, relative to the total number of sporulating cells that contained SpoIIIE-GFP signal (foci or diffuse) in the membranes of the forespore. n>950 per time-course, per strain, per replicate.

- Quantification of GFP-SpoIIIM (Fig. 6F): the percentage of cells with a GFP-SpoIIIM focus (average frequency ± SD of 3 biological replicates) was calculated based on the number of sporulating cells that contained GFP signal (focus or band), relative to the total number of sporulating cells that had progressed into or beyond asymmetric division. $n$>750 per time-course, per strain, per replicate.

The MicrobeJ plugin (Ducret et al., 2016) designed for the Fiji software was used to detect the signal intensity of SpoIIIE-GFP foci (Fig. 2E), on background subtracted images (Process > Subtract Background) to avoid false positive detections of the fluorescent signal. To determine the signal intensity of SpoIIIE-GFP foci, the brightfield image was set to Channel 1 and the image with the GFP signal to Channel 2. These channels were then merged into one image. For Channel 1 of the image with "Bright" background, the "Bacteria" tab was set to "Fit Shape" and "Rod-Shaped" to detect the bacteria in the brightfield image. Five parameters: "Exclude on Edges", "Shape descriptors", "Segmentation", "Intensity", and "Feature" were checked on. To refine the generated bacteria outlines, the shape descriptors (area, length, and width) were set differently for each time-point corresponding to the contours of individual cell. To resolve unprocessed cells, the manual editing tool was also used. For Channel 2 of the image with "Dark" background, the "Maxima" tab was set to "Point" and "Basic". The tolerance was set to 15, and the intensity was set from 15-max to ensure detection of the GFP foci with a minimum signal intensity of 15. Three parameters: "Exclude on Edges", "Shape descriptors", and "Associations" were checked on. The raw data were displayed on a MicrobeJ results table, which was then exported into Excel for data collation and graph generation.

## Supplementary Material

Refer to Web version on PubMed Central for supplementary material.

## Acknowledgments

## References

BARRE FX 2007. FtsK and SpoIIIE: the tale of the conserved tails. Mol Microbiol, 66, 1051–1055. [PubMed: 17973909]

BEN-YEHUDA S, RUDNER DZ & LOSICK R 2003. Assembly of the SpoIIIE DNA translocase depends on chromosome trapping in Bacillus subtilis. Curr Biol, 13, 2196–2200. [PubMed: 14680637]

BESPROZVANNAYA M, PIVORUNAS VL & BURTON BM 2014. Mechanistic study of classical translocation-dead SpoIIIE36 reveals the functional importance of the hinge within the SpoIIIE motor. Journal of Bacteriology, 196, 2481–2490. [PubMed: 24769697]

BESPROZVANNAYA M, PIVORUNAS VL, FELDMAN Z & BURTON BM 2013. SpoIIIE protein achieves directional DNA translocation through allosteric regulation of ATPase activity by an accessory domain. Journal of Biological Chemistry, 288, 28962–28974.

BLAYLOCK B, JIANG X, RUBIO A, MORAN CP JR. & POGLIANO K 2004. Zipper-like interaction between proteins in adjacent daughter cells mediates protein localization. Genes Dev, 18, 2916–2928. [PubMed: 15574594]

BRODER DH & POGLIANO K 2006. Forespore Engulfment Mediated by a Ratchet-Like Mechanism. Cell, 126, 917–928. [PubMed: 16959571]

BUIST G, STEEN A, KOK J & KUIPERS OP 2008. LysM, a widely distributed protein motif for binding to (peptido)glycans. Molecular Microbiology, 68, 838–847. [PubMed: 18430080]

BURTON B & DUBNAU D 2010. Membrane-associated DNA transport machines. Cold Spring Harb Perspect Biol.

BURTON BM, MARQUIS KA, SULLIVAN NL, RAPOPORT TA & RUDNER DZ 2007. The ATPase SpoIIIE Transports DNA across Fused Septal Membranes during Sporulation in Bacillus subtilis. Cell, 131, 1301–1312. [PubMed: 18160039]

CATTONI DI, CHARA O, GODEFROY C, MARGEAT E, TRIGUEROS S, MILHIET PE & NÖLLMANN M 2013. SpoIIIE mechanism of directional translocation involves target search coupled to sequence-dependent motor stimulation. EMBO Reports, 14, 473–479. [PubMed: 23559069]

CATTONI DI, THAKUR S, GODEFROY C, LE GALL A, LAI-KEE-HIM J, MILHIET PE, BRON P & NOLLMANN M 2014. Structure and DNA-binding properties of the Bacillus subtilis SpoIIIE DNA translocase revealed by single-molecule and electron microscopies. Nucleic Acids Res, 42, 2624–2636. [PubMed: 24297254]

CHASTANET A & LOSICK R 2007. Engulfment during sporulation in Bacillus subtilis is governed by a multi-protein complex containing tandemly acting autolysins. Molecular Microbiology, 64, 139–152. [PubMed: 17376078]

CHO H, MCMANUS HR, DOVE SL & BERNHARDT TG 2011. Nucleoid occlusion factor SlmA is a DNA-activated FtsZ polymerization antagonist. Proc Natl Acad Sci U S A, 108, 3773–3778. [PubMed: 21321206]

DOAN T 2013. FisB mediates membrane fission during sporulation in bacillus subtilis. Genes & Development, 10.1101/gad.209049.112.during, 322–334. [PubMed: 23388828]

DOAN T, COLEMAN J, MARQUIS KA, MEESKE AJ, BURTON BM, KARATEKIN E & RUDNER DZ 2013. FisB mediates membrane fission during sporulation in Bacillus subtilis. Genes Dev, 27, 322–334. [PubMed: 23388828]

DOAN T, MORLOT C, MEISNER J, SERRANO M, HENRIQUES AO, MORAN CP & RUDNER DZ 2009. Novel secretion apparatus maintains spore integrity and developmental gene expression in Bacillus subtilis. PLoS Genetics, 5.

DUCRET A, QUARDOKUS EM & BRUN YV 2016. MicrobeJ, a tool for high throughput bacterial cell detection and quantitative analysis. Nat Microbiol, 1, 16077. [PubMed: 27572972]

EICHENBERGER P, JENSEN ST, CONLON EM, VAN OOIJ C, SILVAGGI J, GONZÁLEZ-PASTOR JE, FUJITA M, BEN-YEHUDA S, STRAGIER P, LIU JS & LOSICK R 2003. The σEregulon and the identification of additional sporulation genes in Bacillus subtilis. Journal of Molecular Biology, 327, 945–972. [PubMed: 12662922]

FICHE JB, CATTONI DI, DIEKMANN N, LANGERAK JM, CLERTE C, ROYER CA, MARGEAT E, DOAN T & NÖLLMANN M 2013. Recruitment, Assembly, and Molecular Architecture of the SpoIIIE DNA Pump Revealed by Superresolution Microscopy. PLoS Biology, 11.

FLEMING TC, SHIN JY, LEE SH, BECKER E, HUANG KC, BUSTAMANTE C & POGLIANO K 2010. Dynamic SpoIIIE assembly mediates septal membrane fission during Bacillus subtilis sporulation. Genes and Development, 24, 1160–1172. [PubMed: 20516200]

FRASCHINI R 2020. Cytokinesis in Eukaryotic Cells: The Furrow Complexity at a Glance. Cells, 9.

GRAINGE I 2010. FtsK - a bacterial cell division checkpoint? Molecular Microbiology, 78, 1055–1057. [PubMed: 21155139]

HAJDUK IV, MANN R, RODRIGUES CDA & HARRY EJ 2019. The ParB homologs, Spo0J and Noc, together prevent premature midcell Z ring assembly when the early stages of replication are blocked in Bacillus subtilis. Mol Microbiol, 112, 766–784. [PubMed: 31152469]

HILBERT DW, CHARY VK & PIGGOT PJ 2004. Contrasting Effects of σE on Compartmentalization of σF Activity during Sporulation of Bacillus subtilis. Journal of Bacteriology, 186, 1983–1990. [PubMed: 15028681]

KARIMOVA G, PIDOUX J, ULLMANN A & LADANT D 1998. A bacterial two-hybrid system based on a reconstituted signal transduction pathway. Proc Natl Acad Sci U S A, 95, 5752–5756. [PubMed: 9576956]

KHANNA K, LOPEZ-GARRIDO J & POGLIANO K 2020. Shaping an Endospore: Architectural Transformations During Bacillus subtilis Sporulation. Annu Rev Microbiol, 10.1146/annurev-micro-022520-074650.

KHANNA K, LOPEZ-GARRIDO J, ZHAO Z, WATANABE R, YUAN Y, SUGIE J, POGLIANO K & VILLA E 2019. The molecular architecture of engulfment during Bacillus subtilis sporulation. Elife, 8.

KOO BM, KRITIKOS G, FARELLI JD, TODOR H, TONG K, KIMSEY H, WAPINSKI I, GALARDINI M, CABAL A, PETERS JM, HACHMANN AB, RUDNER DZ, ALLEN KN, TYPAS A & GROSS CA 2017. Construction and Analysis of Two Genome-Scale Deletion Libraries for Bacillus subtilis. Cell Syst, 4, 291–305 e297. [PubMed: 28189581]

LESAGE G & BUSSEY H 2006. Cell wall assembly in Saccharomyces cerevisiae. Microbiol Mol Biol Rev, 70, 317–343. [PubMed: 16760306]

LIU NJL, DUTTON RJ & POGLIANO K 2006. Evidence that the SpoIIIE DNA translocase participates in membrane fusion during cytokinesis and engulfment. Molecular Microbiology, 59, 1097–1113. [PubMed: 16430687]

LOPEZ-GARRIDO J, OJKIC N, KHANNA K, WAGNER FR, VILLA E, ENDRES RG & POGLIANO K 2018. Chromosome Translocation Inflates Bacillus Forespores and Impacts Cellular Morphology. Cell, 172, 758–770.e714. [PubMed: 29425492]

MARQUIS KA, BURTON BM, NOLLMANN M, PTACIN JL, BUSTAMANTE C, BEN-YEHUDA S & RUDNER DZ 2008. SpoIIIE strips proteins off the DNA during chromosome translocation. Genes & development, 22, 1786–1795. [PubMed: 18593879]

MCPHERSON DC, DRIKS A & POPHAM DL 2001. Two Class A High-Molecular-Weight Penicillin-Binding Proteins of. 183, 6046–6053.

MEESKE J, RODRIGUES C, BRADY J, LIM HC, BERNHARDT TG & RUDNER DZ 2016. High-Throughput Genetic Screens Identify a Large and Diverse Collection of New Sporulation Genes in Bacillus subtilis. PLoS Biology, 14, 1–33.

MORLOT C, UEHARA T, MARQUIS KA, BERNHARDT TG & RUDNER DZ 2010. A highly coordinated cell wall degradation machine governs spore morphogenesis in Bacillus subtilis. Genes and Development, 24, 411–422. [PubMed: 20159959]

OJKIC N, LÓPEZ-GARRIDO J, POGLIANO K & ENDRES RG 2014. Bistable Forespore Engulfment in Bacillus subtilis by a Zipper Mechanism in Absence of the Cell Wall. PLoS Computational Biology, 10.

OJKIC N, LÓPEZ-GARRIDO J, POGLIANO K & ENDRES RG 2016. Cell-wall remodeling drives engulfment during Bacillus subtilis sporulation. eLife, 5, 1–30.

PEREZ AR, ABANES-DE MELLO A & POGLIANO K 2000. SpoIIB localizes to active sites of septal biogenesis and spatially regulates septal thinning during engulfment in Bacillus subtilis. Journal of Bacteriology, 182, 1096–1108. [PubMed: 10648537]

PIGGOT PJ & HILBERT DW 2004. Sporulation of Bacillus subtilis. Current Opinion in Microbiology, 7, 579–586. [PubMed: 15556029]

PTACIN JL, NOLLMANN M, BECKER EC, COZZARELLI NR, POGLIANO K & BUSTAMANTE C 2008. Sequence-directed DNA export guides chromosome translocation during sporulation in Bacillus subtilis. Nature Structural and Molecular Biology, 15, 485–493.

RODRIGUES CDA, MARQUIS KA, MEISNER J & RUDNER DZ 2013. Peptidoglycan hydrolysis is required for assembly and activity of the transenvelope secretion complex during sporulation in Bacillus subtilis. Molecular Microbiology, 89, 1039–1052. [PubMed: 23834622]

RODRIGUES C, HENRY X, NEUMANN E, KURAUSKAS V, BELLARD L, FICHOU Y, SCHANDA P, SCHOEHN G, RUDNER DZ & MORLOT C 2016. A ring-shaped conduit connects the mother cell and forespore during sporulation in Bacillus subtilis. Proceedings of the National Academy of Sciences, 113, 11585–11590.

SCHINDELIN J, ARGANDA-CARRERAS I, FRISE E, KAYNIG V, LONGAIR M, PIETZSCH T, PREIBISCH S, RUEDEN C, SAALFELD S, SCHMID B, TINEVEZ JY, WHITE DJ, HARTENSTEIN V, ELICEIRI K, TOMANCAK P & CARDONA A 2012. Fiji: an open-source platform for biological-image analysis. Nat Methods, 9, 676–682. [PubMed: 22743772]

SEILER S & JUSTA-SCHUCH D 2010. Conserved components, but distinct mechanisms for the placement and assembly of the cell division machinery in unicellular and filamentous ascomycetes. Mol Microbiol, 78, 1058–1076. [PubMed: 21091496]

SHARP MD & POGLIANO K 1999. An in vivo membrane fusion assay implicates SpoIIIE in the final stages of engulfment during Bacillus subtilis sporulation. Proceedings of the National Academy of Sciences, 96, 14553–14558.

SHARP MD & POGLIANO K 2002. Role of cell-specific SpoIIIE assembly in polarity of DNA transfer. Science (New York, N.Y.), 295, 137–139.

SHERRATT DJ, ARCISZEWSKA LK, CROZAT E, GRAHAM JE & GRAINGE I 2010. The Escherichia coli DNA translocase FtsK.

STRAGIER P & LOSICK R 1996. Molecular Genetics of Sporulation in Bacillus Subtilis. Annu. Rev. Genet, 30, 297–341. [PubMed: 8982457]

SULLIVAN NL, MARQUIS KA & RUDNER DZ 2009. Recruitment of SMC by ParB-parS organizes the origin region and promotes efficient chromosome segregation. Cell, 137, 697–707. [PubMed: 19450517]

TOCHEVA EI, LÓPEZ-GARRIDO J, HUGHES HV, FREDLUND J, KURU E, VANNIEUWENHZE MS, BRUN YV, POGLIANO K & JENSEN GJ 2013. Peptidoglycan transformations during Bacillus subtilis sporulation. 88, 673–686.

UNIPROT CONSORTIUM T 2018. UniProt: the universal protein knowledgebase. Nucleic Acids Res, 46, 2699. [PubMed: 29425356]

WANG X, MONTERO LLOPIS P & RUDNER DZ 2014. Bacillus subtilis chromosome organization oscillates between two distinct patterns. Proc Natl Acad Sci U S A, 111, 12877–82. [PubMed: 25071173]

WU LJ & ERRINGTON J 1997. Septal localization of the SpoIIIE chromosome partitioning protein in Bacillus subtilis. EMBO Journal, 16, 2161–2169.

WU LJ & ERRINGTON J 1998. Use of asymmetric cell division and spoIIIE mutants to probe chromosome orientation and organization in Bacillus subtilis. Molecular Microbiology, 27, 777–786. [PubMed: 9515703]

YEN SHIN J, LOPEZ-GARRIDO J, LEE S-H, DIAZ-CELIS C, FLEMING T, BUSTAMANTE C & POGLIANO K 2015. Visualization and functional dissection of coaxial paired SpoIIIE channels across the sporulation septum. 10.7554/eLife.06474.001.

ZEIGLER DR, PRÁGAI Z, RODRIGUEZ S, CHEVREUX B, MUFFLER A, ALBERT T, BAI R, WYSS M & PERKINS JB 2008. The origins of 168, W23, and other Bacillus subtilis legacy strains. Journal of Bacteriology, 190, 6983–6995. [PubMed: 18723616]
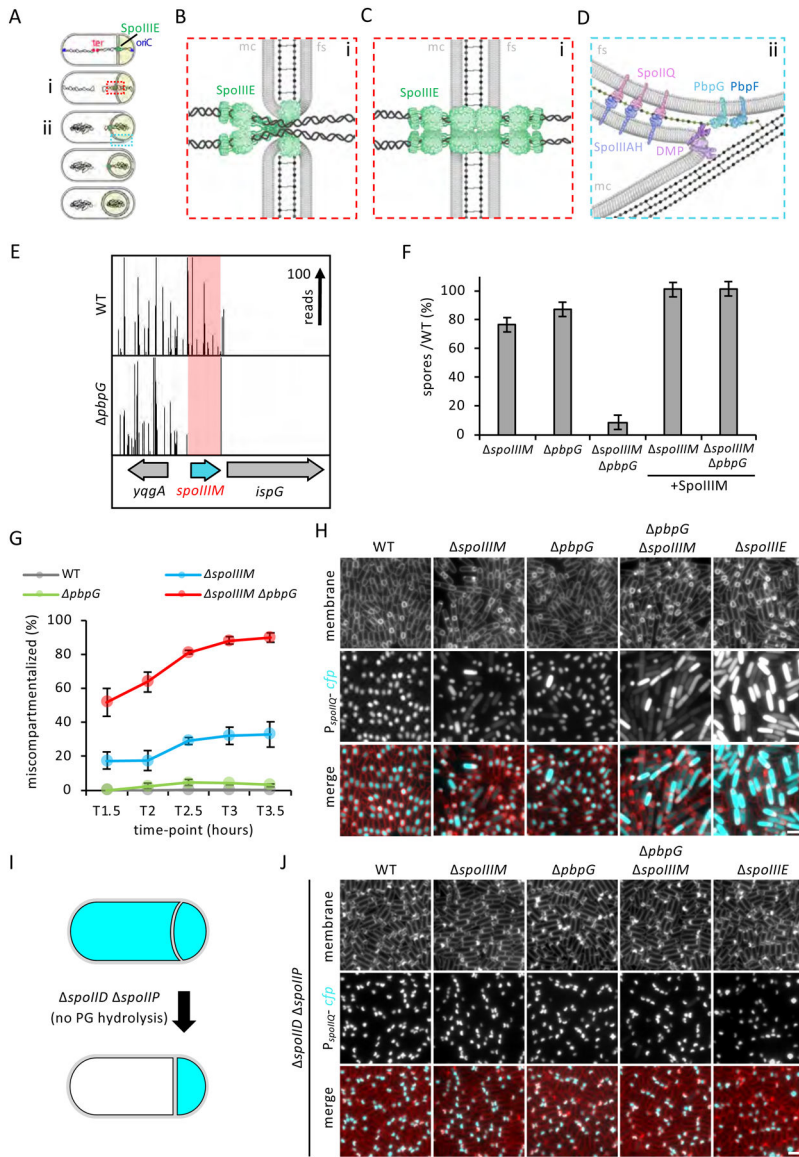
**Figure 1: Identification of SpoIIIM and its requirement, together with PbpG, in maintaining compartmentalization.**

**(A)** Diagram of chromosome translocation and the different stages of engulfment, showing membranes (black), PG (grey), chromosome (black squiggles), SpoIIIE (green), origin (oriC, blue) and terminus (ter, red). The forespore cytoplasm is shown in beige. **(B)** Diagram of Aqueous Pore Model (zoomed-in from red box in Ai), showing SpoIIIE on the mother cell (mc) side and not on the forespore (fs) side, localized within unfused septal membranes that form a pore in the membrane. **(C)** Diagram of Channel Model (zoomed-in from red box in Ai), showing SpoIIIE on both sides of the fused septal membranes. **(D)** Diagram of the leading edge of the engulfing membranes (zoomed-in from blue box in Aii), showing the SpoIIIAH-SpoIIQ interaction across the engulfing membranes, PbpG (light teal) and PbpF (dark teal) in the forespore membrane, the DMP complex (purple), new PG (green dots and lines) and PG in the lateral wall of the sporangium (grey dots and lines). **(E)** Tn-seq profiles in WT and *pbpG* after 24 hours of growth and sporulation in exhaustion medium. The

height of each line reflects the number of sequencing reads at this position. Red box highlights the *spoIIIM* (*yqfZ*) locus, which is depleted for transposon insertions in the *pbpG* library compared to WT. **(F)** Average sporulation efficiency (% ± SD, n=3) of *spoIIIM*, *pbpG*, *spoIIIM pbpG* and the respective *spoIIIM* complementation strains, *spoIIIM* and *pbpG spoIIIM* in DSM medium. **(G)** Average frequency (± SD of 3 biological replicates) of miscompartmentalized cells during a sporulation time-course in WT, *spoIIIM*, *pbpG* and *spoIIIM pbpG* (*n*>900 per time-course, per strain, per replicate). **(H)** Representative images of miscompartmentalization in WT, *spoIIIM*, *pbpG*, *spoIIIM pbpG* and *spoIIIE* at T3.5 (related to Figure 1G). Scale bar, 2 μM. **(I)** Diagram showing the engulfment block occurring in the *spoIID spoIIP* and its effect on compartmentalization by preventing PG hydrolysis. **(J)** Representative images (from one biological replicate, out of 3 examined) of miscompartmentalization in *spoIID spoIIP* at T3.5, in WT, *spoIIIM*, *pbpG*, *spoIIIM pbpG* and *spoIIIE* backgrounds. Scale bar, 2 μM.
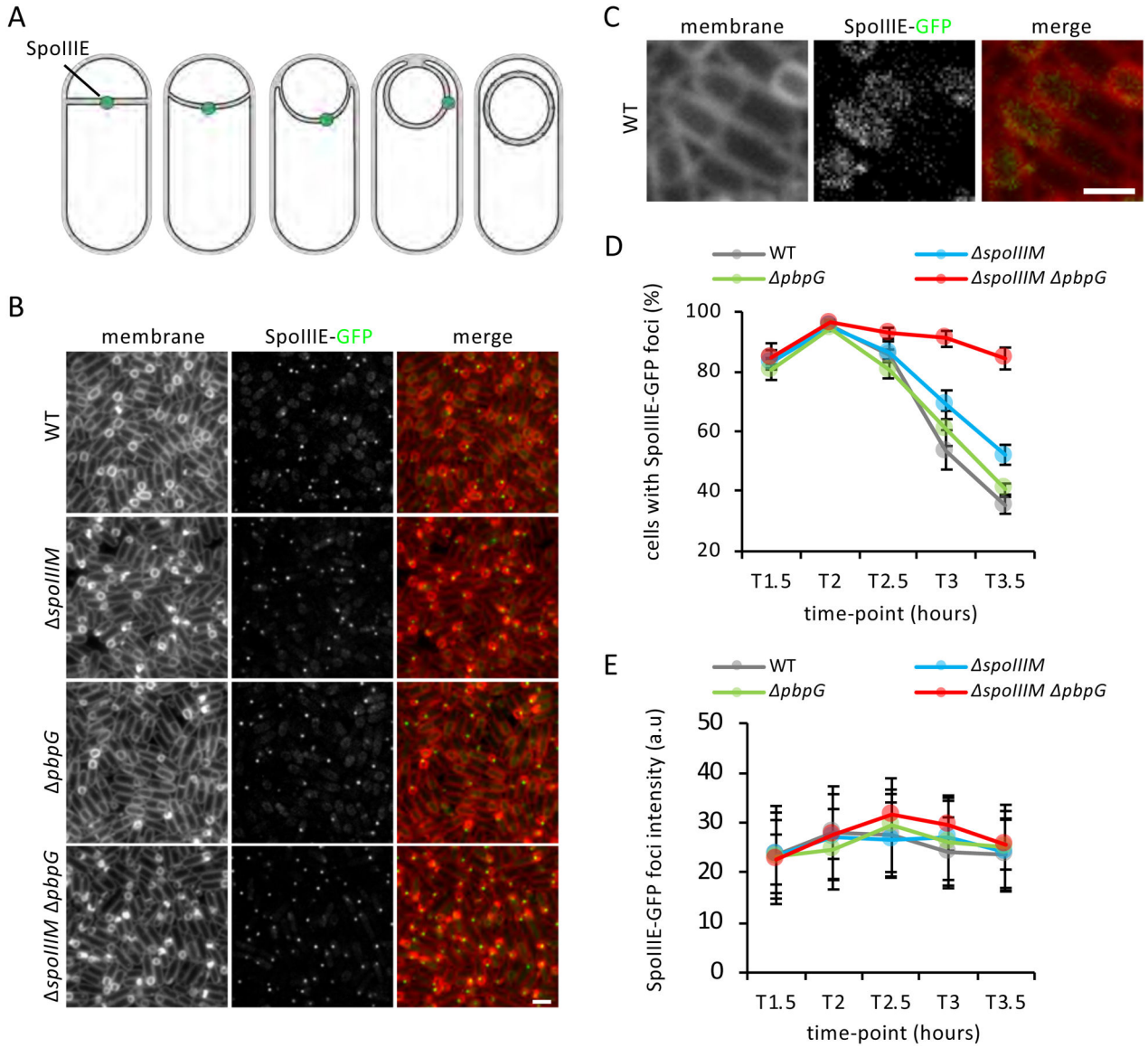
**Figure 2: SpoIIIE foci persist in the absence of SpoIIIM and PbpG.**

**(A)** Diagram showing the dynamic localization of SpoIIIE during engulfment. **(B)** Representative images of the localization of SpoIIIE-GFP in WT, *spoIIIM*, *pbpG* and *spoIIIM pbpG* at T3.5. Scale bar, 2 μM. **(C)** Representative image of the diffused localization of SpoIIIE in WT cells that have completed engulfment. Scale bar, 1 μM. **(D)** Average frequency (± SD of of 3 biological replicates) of cells with SpoIIIE-GFP foci in WT, *spoIIIM*, *pbpG* and *spoIIIM pbpG* during a sporulation time-course (n>1000 per time-course, per strain, per replicate). **(E)** Average fluorescence (± STDEVP, n>400, per time-point, per strain) intensity of SpoIIIE-GFP foci in WT, *spoIIIM*, *pbpG* and *spoIIIM pbpG* during a sporulation time-course.
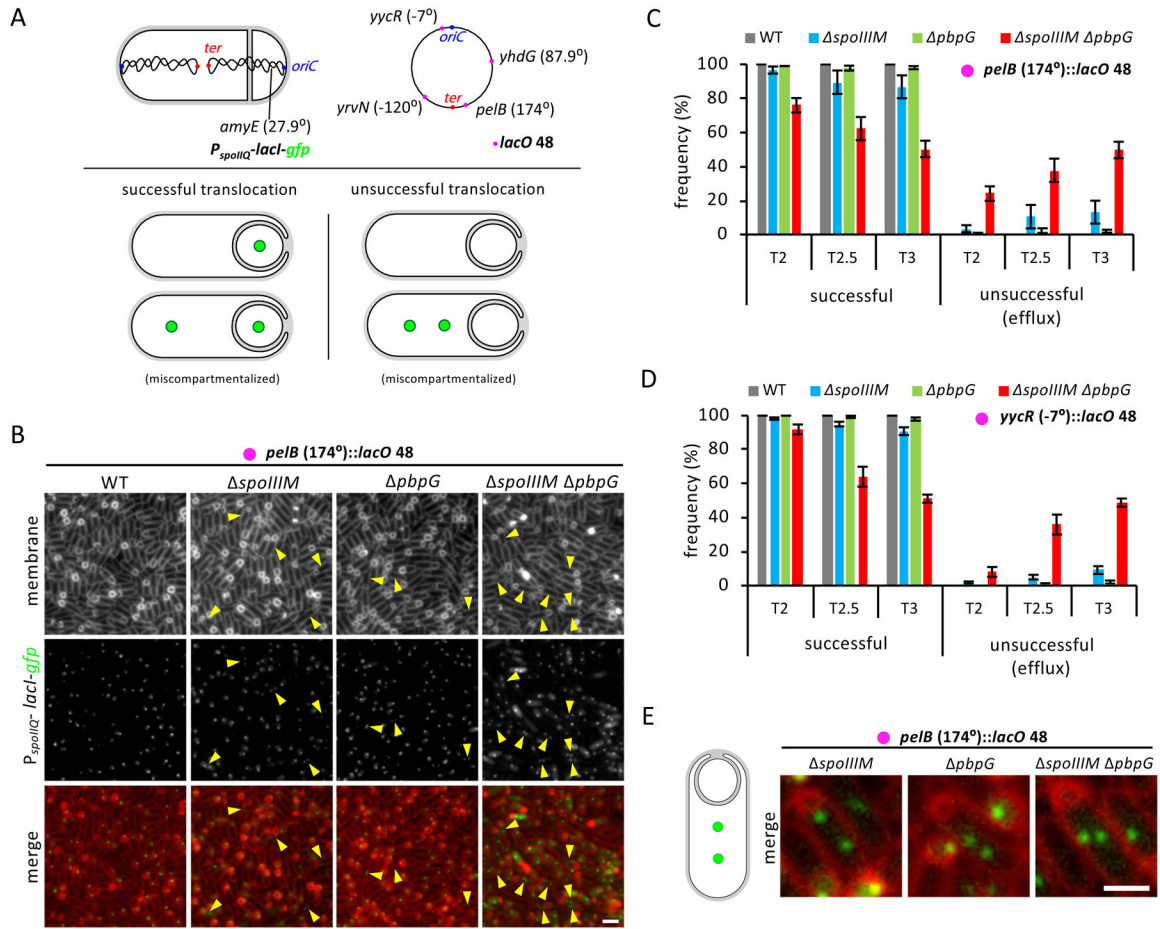
**Figure 3: Efficient chromosome translocation requires SpoIIIM and PbpG.**
(**A**) Diagram explaining experimental rationale of the LacI-*lacO* system for visualizing chromosome translocation. LacI-GFP, expressed in the forespore (P$_{spoIIQ}$) from the *amyE* locus, binds to *lacO48* sites inserted at the *yhdG*, *pelB*, *yrvN* or *yycR* chromosomal locus. The origin (*oriC*) and terminus (*ter*) loci are shown in blue and red, respectively. Successful chromosome translocation is indicated by a LacI-GFP focus in the forespore, with an additional focus in the mother cell compartment in the event of miscompartmentalization. Unsuccessful chromosome translocation is indicated by an absence of LacI-GFP foci, or by two LacI-GFP foci in the mother cell compartment in the event of miscompartmentalization. (**B**) Representative images of LacI-GFP foci at T3 in WT, *spoIIIM*, *pbpG* and *spoIIIM pbpG* strains containing *lacO48* inserted at the *pelB* locus (174°). Yellow arrowheads point to cells with two mother cell foci. Scale bar, 2 μM. (**C**) Average frequency (± SD of 3 biological replicates) of cells with a LacI-GFP focus in the forespore (successful translocation) or with no or two LacI-GFP foci in the mother cell (unsuccessful translocation, efflux) during a sporulation time-course, with *lacO48* integrated at the *pelB* locus (174°) and (**D**) at the *yycR* locus (−7°) in WT, *spoIIIM*, *pbpG* and *spoIIIM pbpG* (*n*>650 per time-course, per strain, per replicate). (**E**) Representative images of cells at T3 with two LacI-GFP foci in the mother cell of *spoIIIM*, *pbpG* and *spoIIIM pbpG* sporulating cells containing *lacO48* inserted at the *pelB* locus (174°).
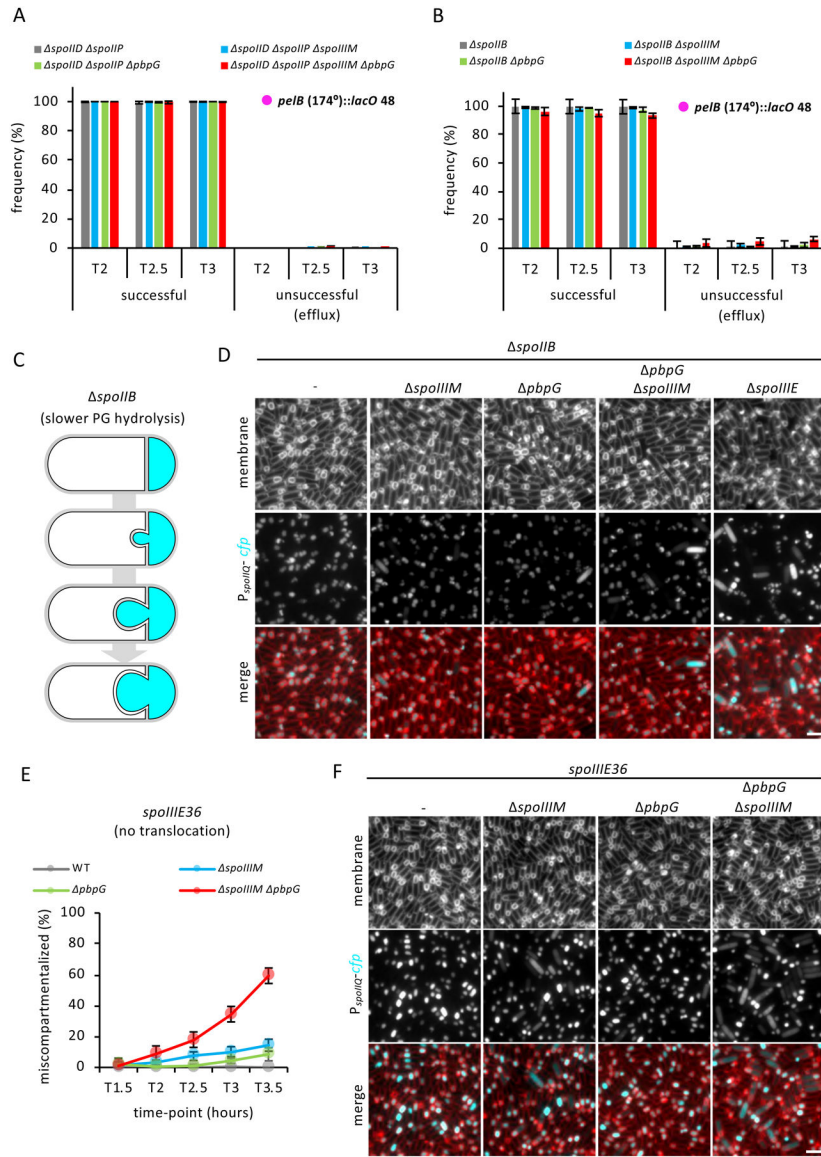
**Figure 4: Blocking or impairing engulfment restores efficient chromosome translocation and compartmentalization in the absence of SpoIIIM and PbpG.**

(**A**) Average frequency (± SD of 3 biological replicates) of cells with a LacI-GFP focus in the forespore or with two LacI-GFP foci in the mother cell during a sporulation time-course, with *lacO 48* integrated at the *pelB* locus (174°) in the *spoIID spoIIP* alone or combined with the *spoIIIM*, *pbpG* and *pbpG spoIIIM* (*n*>600 per time-course, per strain, per replicate). (**B**) Average frequency (± SD of 3 biological replicates) of cells with a LacI-GFP focus in the forespore or with two LacI-GFP foci in the mother cell during a sporulation time-course, with *lacO 48* integrated at the *pelB* locus (174°) in the *spoIIB* alone or combined with the *spoIIIM*, *pbpG* and *spoIIIM pbpG* (*n*>600 per time-course, per strain, per replicate). (**C**) Schematic representation of the slower engulfment and membrane bulging phenotype observed in the *spoIIB*. Cyan represents forespore-specific CFP. (**D**) Representative images of sporulating cells at T3 showing compartmentalization of forespore gene expression in *spoIIB* mutant alone, or combined with the *spoIIIM*, *pbpG*,

*spoIIIM   pbpG* and   *spoIIIE*. Scale bar, 2 μM. **(E)** Average frequency (± SD of 3 biological replicates) of miscompartmentalized cells during a sporulation time-course in the *spoIIIE36* mutant in otherwise WT (grey),   *spoIIIM* (blue),   *pbpG* (green) and   *spoIIIM   pbpG* (red) strains ($n$>750 per time-course, per strain). **(F)** Representative images of miscompartmentalization in the *spoIIIE36* mutant in otherwise WT,   *spoIIIM*,   *pbpG* and   *spoIIIM   pbpG* strains at T3.5. Scale bar, 2 μM.
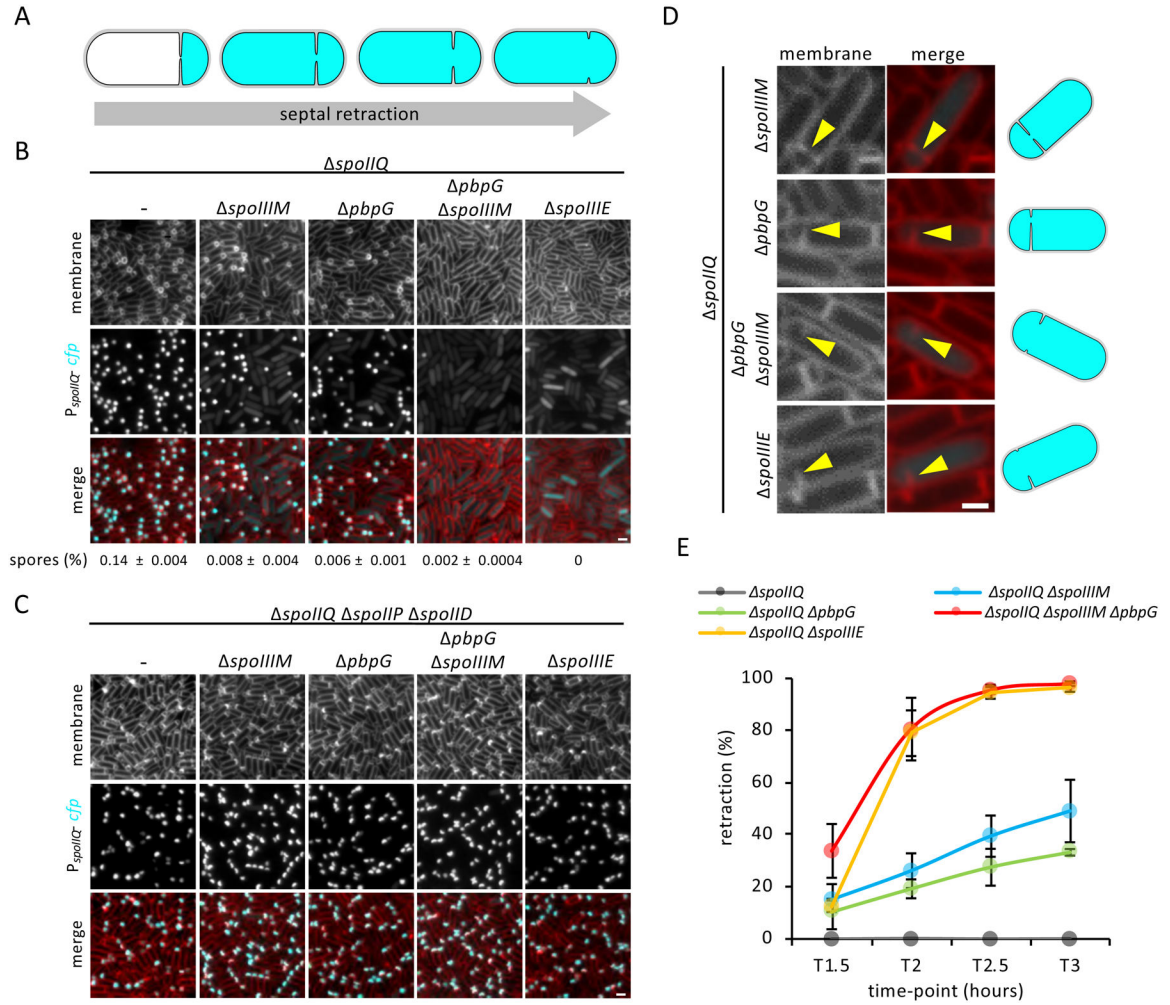
Author Manuscript

Author Manuscript

Author Manuscript

Author Manuscript

**Figure 5: Septa retraction and its dependency on PG hydrolysis.**
**(A)** Schematic representation of septal retraction, illustrating that as septal retraction progresses, CFP fluorescence (cyan) leaks from the forespore to fill the entire cell. **(B)** Representative images of septal retraction in WT, *spoIIIM*, *pbpG*, *spoIIIM pbpG* and *spoIIIE* in a *spoIIQ* background at T3. Scale bar,2 µM. Sporulation efficiency (%, average ± SD, n=3) is shown below the respective strains. **(C)** Representative images of septal retraction suppression in cells blocked for engulfment in WT, *spoIIIM*, *pbpG*, *spoIIIM pbpG* and *spoIIIE* strains at T3. Scale bar, 2 µM. **(D)** Representative zoomed-in examples of septal retraction in *spoIIIM*, *pbpG*, *spoIIIM pbpG* and *spoIIIE* at T3. Yellow arrowheads point to retracting septa. Scale bar,1 µM. Schematic representations of cells are shown on the right. **(E)** Average frequency (± SD of of 3 biological replicates) of cells exhibiting septal retraction in WT, *spoIIIM*, *pbpG*, *spoIIIM pbpG* and *spoIIIE* during a sporulation time-course (*n*>600 per time-point, per strain, per replicate).
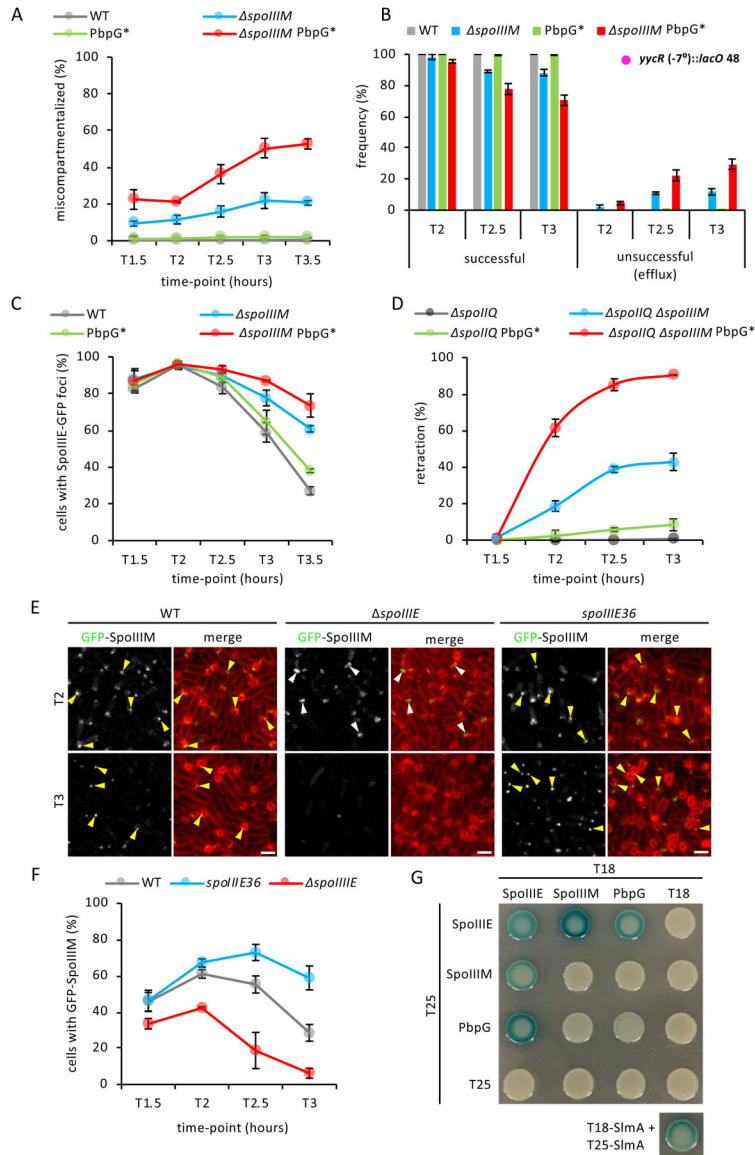
**Figure 6: Peptidoglycan synthesis by PbpG is required for developmental characteristics and evidence that SpoIIIE, SpoIIIM and PbpG form a complex.**

**(A)** Average frequency (± SD of 3 biological replicates) miscompartmentalized cells during a sporulation time-course in WT, *spoIIIM*, *pbpG\** and *spoIIIM pbpG\** strains (*n*>900 per time-course, per strain, per replicate). **(B)** Average frequency (± SD of of 3 biological replicates) of cells with a LacI-GFP focus in the forespore (successful translocation) or with no or two LacI-GFP foci in the mother cell (unsuccessful translocation, efflux) during a sporulation time-course, with *lacO48* integrated at the *yycR* locus (−7°), in WT, *spoIIIM*, PbpG*\** and *spoIIIM* PbpG* (*n*>600 per time-course, per strain, per replicate). **(C)** Average frequency (± SD of 3 biological replicates) of cells with SpoIIIE-GFP foci during a sporulation time-course in WT (grey), *spoIIIM*, PbpG* and *spoIIIM* PbpG* (*n*>950 per time-course, per strain, per replicate). **(D)** Average frequency (± SD of of 3 biological replicates) of sporulating cells exhibiting septal retraction during a sporulation time-course in WT *spoIIIM*, PbpG* and *spoIIIM* PbpG* (*n*>700 per time-course, per strain, per

replicate). **(D)** Representative images of GFP-SpoIIIM localization in WT, *spoIIIE* and *spoIIIE36* strains at T2 and T3. Yellow arrowheads indicate GFP-SpoIIIM fluorescence that appears to disperse, disappear or remain as a stable focus as engulfment nears completion in WT, *spoIIIE* and *spoIIIE36* mutant. Scale bar,2 μM. **(F)** Average frequency (± SD of 3 biological replicates) of cells with GFP-SpoIIIM fluorescence in WT, *spoIIIE* and *spoIIIE36* during sporulation time-course (*n*>750 per time-course, per strain, per replicate). **(G)** Bacterial two-hybrid assay of T18 and T25 fusions to SpoIIIE, SpoIIIM and PbpG. T18-SlmA and T25-SlmA interaction is included as a positive control (Cho et al., 2011).
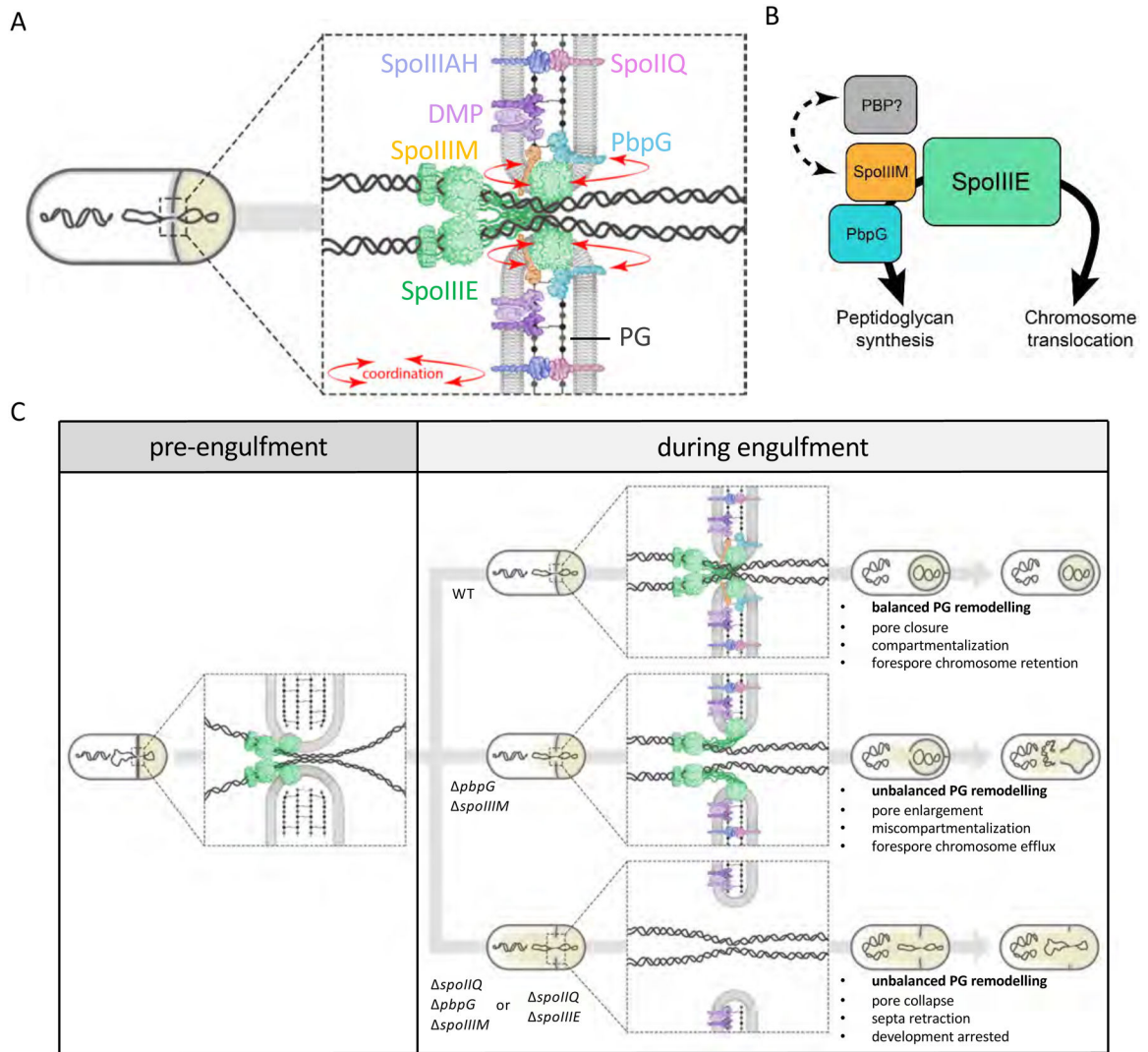
**Figure 7: Model illustrating coordination of PG remodelling and chromosome translocation at a highly-stabilized septal pore.**

**(A)** Schematic illustration showing coordination (red arrows) of chromosome translocation and PG remodelling by SpoIIIM and PbpG *via* SpoIIIE, at the septal pore. **(B)** Interaction network of SpoIIIE, highlighting its role in chromosome translocation and its role in PG synthesis *via* interactions with SpoIIIM and PbpG. We hypothesize that a putative unidentified PG synthase (PBP) may also be involved in PG remodelling *via* interaction with SpoIIIM. **(C)** Schematic representation of the septal membrane, before and after initiation of engulfment and how different molecular components contribute to ensuring developmental compartmentalization and chromosome translocation upon initiation of engulfment. Note that in the *spoIIQ spoIIIM pbpG* triple mutant, SpoIIIE is still present as focus in retracted septa (Fig. S4) but for simplicity this is not shown in the bottom panel.

KEY RESOURCES TABLE

| REAGENT or RESOURCE | SOURCE | IDENTIFIER |
|---|---|---|
| **Antibodies** | | |
| THE™ His Tag Antibody, mAb, Mouse | GenScript | Cat#A00186 |
| anti-FtsZ | (Hajduk et al., 2019) | N/A |
| anti-SpoIIIAG | (Doan et al., 2009) | N/A |
| **Bacterial Strains** | | |
| bBB042 | (Burton et al., 2007) | N/A |
| bBB069 | (Besprozvannaya et al., 2014) | N/A |
| bDR2413 (168) | (Zeigler et al., 2008) | N/A |
| bWX1200 | (Wang et al., 2014) | N/A |
| See Table S1 for a complete list of strains used in this study. | N/A | N/A |
| **Chemicals** | | |
| FM4–64 | Thermo Fisher Scientific | Cat#T13320 |
| SYTOX® Orange | Thermo Fisher Scientific | Cat#S11368 |
| TMA-DPH | Thermo Fisher Scientific | Cat#T204 |
| **Oligonucleotides** | | |
| See Table S2 for a complete list of oligonucleotides used in this study. | Integrated DNA Technologies (IDT) | https://sg.idtdna.com/ |
| **Recombinant DNA** | | |
| $P_{lac}$::T25-slmA (kan) | (Cho et al., 2011) | pHC535 |
| $P_{lac}$::T18-slmA (amp) | (Cho et al., 2011) | pHC538 |
| See Table S3 for a complete list of plasmids constructed for this study. | N/A | N/A |
| **Software and Algorithms** | | |
| Fiji software | (Schindelin et al., 2012) | https://imagej.net/Welcome |
| MicrobeJ | (Ducret et al., 2016) | https://www.microbej.com/ |